AFRL-VS-HA-TR-2006-1069

Characterization of an Explosion Source in a Complex Medium by Modeling and Wavelet Domain Inversion

M. Nafi Toksöz

Earth Resources Laboratory
Dept. of Earth, Atmospheric and Planetary Sciences
Massachusetts Institute of Technology

1 June 2006

Final Report

AIR FORCE RESEARCH LABORATORY
Space Vehicles Directorate
29 Randolph Road
AIR FORCE MATERIEL COMMAND
Hanscom AFB, MA 01731-3010

This technical report has been reviewed and is approved for publication.

AFRL-VS-HA-TR-2006-1069

/signed/

ROBERT J. RAISTRICK
Contract Manager

/signed/

ROBERT BELAND, Chief
Battlespace Surveillance Innovation Center

This report has been reviewed by the ESC Public Affairs Office (PA) and is releasable to the National Technical Information Service (NTIS).

Qualified requestors may obtain additional copies from the Defense Technical Information Center (DTIC). All others should apply to the National Technical Information Service.

If your address has changed, if you wish to be removed from the mailing list, or if the addressee is no longer employed by your organization, please notify AFRL/VSIM, 29 Randolph Rd., Hanscom AFB, MA 01731-3010. This will assist us in maintaining a current mailing list.

Do not return copies of this report unless contractual obligations or notices on a specific document require that it be returned.

Using Government drawings, specifications, or other data included in this document for any purpose other than Government procurement does not in any way obligate the U.S. Government. The fact that the Government formulated or supplied the drawings, specifications, or other data does not license the holder or any other person or corporation; or convey any rights or permission to manufacture, use, or sell any patented invention that may relate to them.

This report is published in the interest of scientific and technical information exchange and its publication does not constitute the Government's approval or disapproval of its ideas or findings.

REPORT DOCUMENTATION PAGE

Form Approved
OMB No. 0704-0188

1. REPORT DATE	2. REPORT TYPE	3. DATES COVERED *(From - To)*
1-Jun-06	Final Report	11 Dec 2003 to 10 Dec 2005

4. TITLE AND SUBTITLE
Characterization of an Explosion Source in a Complex Medium by Modeling and Wavelet Domain Inversion

5a. CONTRACT NUMBER
F19628-03-C-0126

5b. GRANT NUMBER

5c. PROGRAM ELEMENT NUMBER
62601F

6. AUTHOR(S)
Prof. M. Nafi Toksöz

5d. PROJECT NUMBER
1010

5e. TASK NUMBER
SM

5f. WORK UNIT NUMBER
A1

7. PERFORMING ORGANIZATION NAME(S) AND ADDRESS(ES)

Earth Resources Laboratory
Department of Earth, Atmospheric and Planetary Sciences
Massachusetts Institute of Technology
E34-455, 42 Carleton Street
Cambridge, MA 02142

8. PERFORMING ORGANIZATION REPORT NUMBER

9. SPONSORING / MONITORING AGENCY NAME(S) AND ADDRESS(ES)
Air Force Research Laboratory
29 Randolph Road
Hanscom AFB, MA 01731-3010

10. SPONSOR/MONITOR'S ACRONYM(S)
AFRL/VSBYE

11. SPONSOR/MONITOR'S REPORT NUMBER(S)
AFRL-VS-HA-TR-2006-1069

12. DISTRIBUTION / AVAILABILITY STATEMENT
Approved for Public Release; Distribution Unlimited.

13. SUPPLEMENTARY NOTES

14. ABSTRACT Explosions are often conducted in complexes with chambers, tunnels, and shafts used for access and instrumentation. These structures and sharp topographic features can act as strong scatterers of seismic waves and complicate the radiation patterns from explosions. In extreme cases they could affect discrimination between earthquakes and explosions. The objectives of this research are (1) to study the effects of these near-source scatterers on seismic waves radiated from explosions, and (2) to use a wavelet domain based moment-tensor inversion scheme to determine "explosive" and "multi-couple" components of the source. To calculate seismograms from an explosion near strong scatterers we use a new finite difference algorithm that accomplishes variable griding by coordinate transformation or "stretching." This method provides excellent numerical stability while increasing computational efficiency. It is capable of 3-D calculations for sources near strong scatterers in heterogeneous media. Seismograms are calculated to determine effects of various scatterers on seismic radiation patterns. The code is developed for realistic earth models including (1) free surface, (2) layered structure, (3) surface topography, and (4) seismic attenuation. In addition, a perfectly matched layer (PML) was incorporated into the finite-difference code to improve the absorption at the boundaries and for saving memory. Forward modelings using the 3-D finite-difference code are conducted with an explosive source and tunnel in a full space and a layered half-space. Calculations are carried out for each case: (1) a reference model without a tunnel, and (2) a finite length horizontal tunnel included. The calculations show P to P and P to S scattering and a complicated radiation pattern of the wave field. P to S scattering is strong and the tunnel acts as a virtual shear wave source. For the half-space model, surface waves dominate the seismograms and significant SH waves are generated by the presence of the tunnel because of shallow depth. We show the capacity of our code in modeling wave scattering due to various topographical features. The sharp corners of a mesa act as strong scatters of seismic waves, and a smooth hill scatters the waves much less. We use synthetic seismograms to test the performance of moment tensor inversion and its ability to separate the volumetric and shear components of the source. With good azimuthal coverage, the moment tensor shows significant shear components in the presence of a scatterer when surface waves dominate the seismogram. The use of wavelets for moment-tensor inversion has advantages because it can use all or part of a seismogram, and has effective de-noising capability. The method can be used to analyze data from earthquakes and explosions for determining isotropic (explosion) and multi-couple (earthquake) components of the source. This is valuable for seismic discrimination. We test the applicability of Time Reversed Acoustics (TRA) approach for detecting the presence of a tunnel near the source. In this approach, the recorded seismograms are time-reversed and sent back into the earth at each station. The back-propagating wavefields focus at the source. The P wave focuses strongly at the explosion while the S wave at the tunnel. TRA has great potential for determining the seismic source properties.

15. SUBJECT TERMS
Seismic scattering, Seismic source inversion, Seismic time-reversed propagation

16. SECURITY CLASSIFICATION OF:			17. LIMITATION OF ABSTRACT	18. NUMBER OF PAGES	19a. NAME OF RESPONSIBLE PERSON
a. REPORT	b. ABSTRACT	c. THIS PAGE			Robert J. Raistrick
UNCLAS	UNCLAS	UNCLAS	SAR		19b. TELEPHONE NUMBER *(include area code)* 781-377-3726

Table of Contents

List of Figures

1. Summary

Explosions are often conducted in complexes with chambers, tunnels, and shafts used for access and instrumentation. These structures and sharp topographic features can act as strong scatterers of seismic waves and complicate the radiation patterns from explosions. In extreme cases they could affect discrimination between earthquakes and explosions. The objectives of this research are (1) to study the effects of these near-source scatterers on seismic waves radiated from explosions, and (2) to use a wavelet domain based moment-tensor inversion scheme to determine "explosive" and "multi-couple" components of the source.

To calculate seismograms from an explosion near strong scatterers we use a new finite difference algorithm that accomplishes variable griding by coordinate transformation or "stretching." This method provides excellent numerical stability while increasing computational efficiency. It is capable of 3-D calculations for sources near strong scatterers in heterogeneous media. Seismograms are calculated to determine effects of various scatterers on seismic radiation patterns. The code is developed for realistic earth models including (1) free surface, (2) layered structure, (3) surface topography, and (4) seismic attenuation. In addition, a perfectly matched layer (PML) was incorporated into the finite-difference code to improve the absorption at the boundaries and for saving memory. Forward modelings using the 3-D finite-difference code are conducted with an explosive source and tunnel in a full space and a layered half-space. Calculations are carried out for each case: (1) a reference model without a tunnel, and (2) a finite length horizontal tunnel included. The calculations show P to P and P to S scattering and a complicated radiation pattern of the wave field. P to S scattering is strong and the tunnel acts as a virtual shear wave source. For the half-space model, surface waves dominate the seismograms and significant SH waves are generated by the presence of the tunnel because of shallow depth. We show the capacity of our code in modeling wave scattering due to various topographical features. The sharp corners of a mesa act as strong scatters of seismic waves, and a smooth hill scatters the waves much less.

We use synthetic seismograms to test the performance of moment tensor inversion and its ability to separate the volumetric and shear components of the source. With good azimuthal coverage, the moment tensor shows significant shear components in the presence of a scatterer when surface waves dominate the seismogram. The use of wavelets for moment-tensor inversion has advantages because it can use all or part of a seismogram, and has effective de-noising capability. The method can be used to analyze data from earthquakes and explosions for determining isotropic (explosion) and multi-couple (earthquake) components of the source. This is valuable for seismic discrimination.

We test the applicability of Time Reversed Acoustics (TRA) approach for detecting the presence of a tunnel near the source. In this approach, the recorded seismograms are time-reversed and sent back into the earth at each station. The back-propagating wavefields focus at the source. The P wave focuses strongly at the explosion while the S wave at the tunnel. TRA has great potential for determining the seismic source properties.

2. Mechanisms on Scattering due to an Explosive Source

2.1 Observation on Transverse wave generations

An explosive source in a laterally homogeneous layered half-space generates P, SV, and Rayleigh waves, but not SH or Love waves. However, seismograms from a large number of explosions show nonisotropic radiation patterns for P and Rayleigh waves, and prominent SH and Love waves. Various mechanisms have been proposed to explain the generation of these transverse waves.

2.2 Objectives of This Research

In this project, we will study the role of scattering from near source structures such as tunnels, shafts, adits, and surface topography for contributing to the generation of complicated radiation patterns and SH waves from explosions. In addition, we will utilize a wavelet domain moment tensor inversion to separate the isotropic (i.e., explosion) and multi-couple components of the source as an aid to seismic discrimination.

Medium properties near the source, heterogeneities along the propagation paths, and scattering near the receivers (Johnson, 1995) all contribute to complexities of seismic waves recorded from explosions. Path and near receiver effects are unique to each receiver. The near-source complexities, however, affect all seismograms and lead to complicated source functions that affect the important task of discriminating between earthquakes and explosions.

The near-source contribution to nonisotropic radiation of P, Rayleigh waves and SH wave generation by an explosion can be attributed to three mechanisms. First, is the tectonic strain energy released by the explosion, resulting in a composite source consisting of an explosion and a double couple (e.g., Archambeau and Wqmmiw, 1970; Toksöz *et al.*, 1965; Toksöz and Kehrer, 1972; Wallace *et al.*, 1983, 1985; Priestley *et al.*, 1990; Schlittenhardt, 1991; Stump *et al.*, 1994; Patton and Taylor, 1995). Tectonic strain release, widely observed for explosions in competent rock, has a greater contribution at low frequencies than at high frequencies.

The second factor that contributes to nonisotropic seismic radiation pattern from explosive sources is the shape of the explosion cavity, and the location of explosive source in that cavity (Rial, and Moran, 1986; Stevens et al., 1991; Zhao and Harkrider, 1992; Ben-Menahem and Mikhailov, 1995; Gibson et al., 1996; Ben-Menahem, 1997; Imhof and Toksöz, 2002;). The contribution of this mechanism to nonisotropic radiation depends on the aspect ratio of the cavity (i.e., ratio of length to diameter), and placement of the source within the cavity (Gibson et al., 1996). To have a significant effect, a very large aspect ratio or a source placed in one end of a long cylindrical cavity was required. Stevens et al. (1991) examined the effects of an ellipsoidal cavity. Their conclusion was that at frequencies of 1 Hz or less, the P-wave radiation pattern was nearly isotropic and the S-wave amplitudes were small.

The third mechanism contributing to complex seismic radiation from an explosion is the near source scattering (Gupta et al., 1990; Johnson, 1997; Ben-Menahem, 1997; Imhof and Toksöz, 2002, 002). This mechanism, not studied as extensively, could be significant when strong scatterers are present near the source. The first task of the proposed research is this near source scattering mechanism.

2.3. Effect of Near Source Scattering on Seismic Waves from Explosions

Explosions often take place in complexes with chambers, shafts, and tunnels used for access and instrumentation (Denny and Stull, 1994; Murphy et al., 1994). Cavities and tunnels can act as strong scatterers and efficiently convert different wave-types into each other (Tadeu et al., 1996). The scatterers act as secondary sources with difference radiation patterns and different distance dependencies than the primary waves. A large amount of S wave energy can be generated by this mechanism by an explosion (Leavy, 1993; Ben-Menahem, 1997; Imhof and Toksöz, 2000, 2002).

Imhof and Toksöz (2000, 2002) modeled the effects of scattering from cylindrical cavities near a shot using a multiple-multipole approximation. Their results showed scattering affected the P-wave radiation pattern and generated significant S waves. Because of the limitation of the method, these studies were limited to 2D geometry, with infinitely long cylinders for sources and scatterers.

To evaluate the effects of scattering realistically, one needs to solve the 3D problem consisting of explosive sources, finite dimension scatterers of various shapes (e.g., cylinders), and a free surface. This is a formidable numerical problem, but can be done with an appropriate numerical approach. For this we will use a new finite difference algorithm described below.

3. Application of Finite Difference Modeling in Studying Wave Propagation

3.1 Finite Difference with Coordinate Stretching

The finite difference time domain method (FDTD) is one of the most widely used tools to simulate wave propagations in 2-D and 3-D elastic media with general spatial variations of elastic properties. While efficiency can be achieved by sampling the physical space adaptively with a variable grid, this benefit may be offset by problems introduced by change in grid size. Wave distortion or numerical reflections may occur due to phase change at the interface of two grids (Browning et al., 1973). Numerical reflections can be eliminated by taking extra averages of solutions at the grid interface, however wave distortion cannot always be avoided. It is also hard to match and implement finite difference approximations at the interface of different grids (Lilla, 1997; Hayashi, 1999). Introducing a change in grid spacing may adversely affect the formal truncation error and the stability of the system (Crowder and Dalton, 1971). By counting phase shift on a nonuniform spacing grid, a 3D elastic FDTD approach was developed to avoid numerical reflections and reduce wave distortions (Pitarka, 1999).

Pitarka's approach requires solving a linear system before conducting the FDTD calculation. The linear system must be solved again when changing the difference operator (e.g., from 4th to 8th order). To avoid doing this, we apply a coordinate transformation, or stretching, to achieve effective variable griding in the physical domain and uniform griding in the transformed domain. Because the computation is carried out on a uniform grid, the formal truncation error and the stability properties of the finite

difference computation are preserved. In addition, numerical implementation becomes easier and more flexible.

A further increase in computational efficiency and accuracy is achieved by employing a wavelet-based difference operator. At the same accuracy, the wavelet-based FDTD scheme allows eight times more coarse sampling for 3-D models than the popular 4th order method, and is comparable to higher order (6th/8th) schemes. At discontinuities, the wavelet-based approach outperforms the 2nd, 4th, 6th and 8th order Taylor's expansion-based schemes, especially when combined with variable griding in the neighborhood of a discontinuity.

3.2 Test of Scattering Due to a Near-Source Cavity in 2-Dimension

As a test and also the first step of this research, strong scattering from the near source cavity is simulated with the FDTD algorithm described above. The model is 2400 m X 2400 m in the x and y direction, and infinite in the z direction. An explosion source with center frequency of 10 Hz is placed in the center of the model. The cavity is an infinite cylinder full of air, and has a radius of 10 m. The distance between the source and the cavity is 100 m. The compressional and shear velocities are 2000 m/s and 1000 m/s, respectively. Grid size for the solid domain is 10 m and 1 m for the cavity area. A smooth transition zone of 10 m is applied between the fine and coarse grid area to further reduce grid-induced reflection. The size of the constructed mesh is 284 × 284. Figures 1a and 1b show the model setup and griding details close to the cavity.

Two snapshots of the stress component (T_{xx}) are shown in Figures 2a,b. These show the interaction of the waves with the cylindrical cavity. The cavity acts as a secondary source (Figure 2b) radiating both P and S waves.

Figures 3a,b and 4a,b show seismograms as a function of azimuth at two horizontal planes located 100 m and 500 m above the source, respectively. The effect of the cavity alters the azimuthal isotropy of P-waves radiation. Also, there is a small azimuth dependent tangential component to P-waves. The SH-wave radiation pattern (Figures 3b and 4b) is more complicated than that of a double couple.

As part of the work, we upgraded the program from 2.5 dimensions to three dimensions. With 3D calculations, scatterers with different shapes and orientations,

velocity variation in the medium, and free surface effects can be modeled. The original program was only capable for 2.5 dimensions because of limitation of computer resources. A new computer cluster with 24 CPUs facilitated the 3D computation.

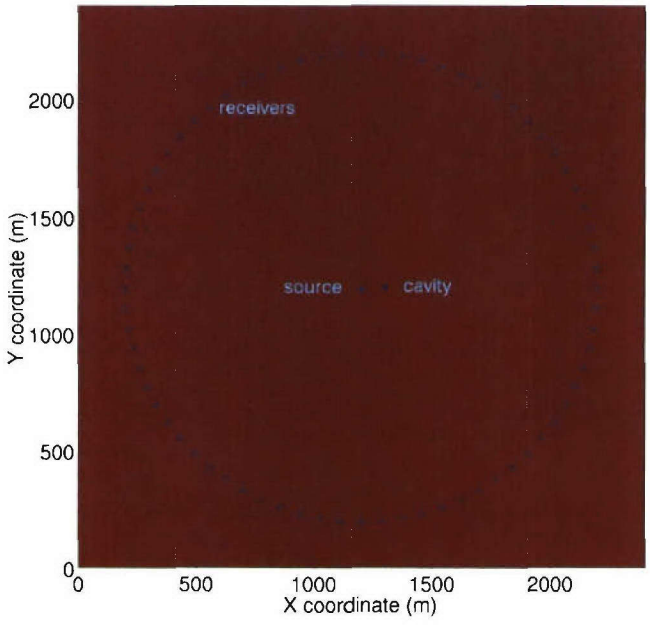

Figure 1a. Model setup and station map.

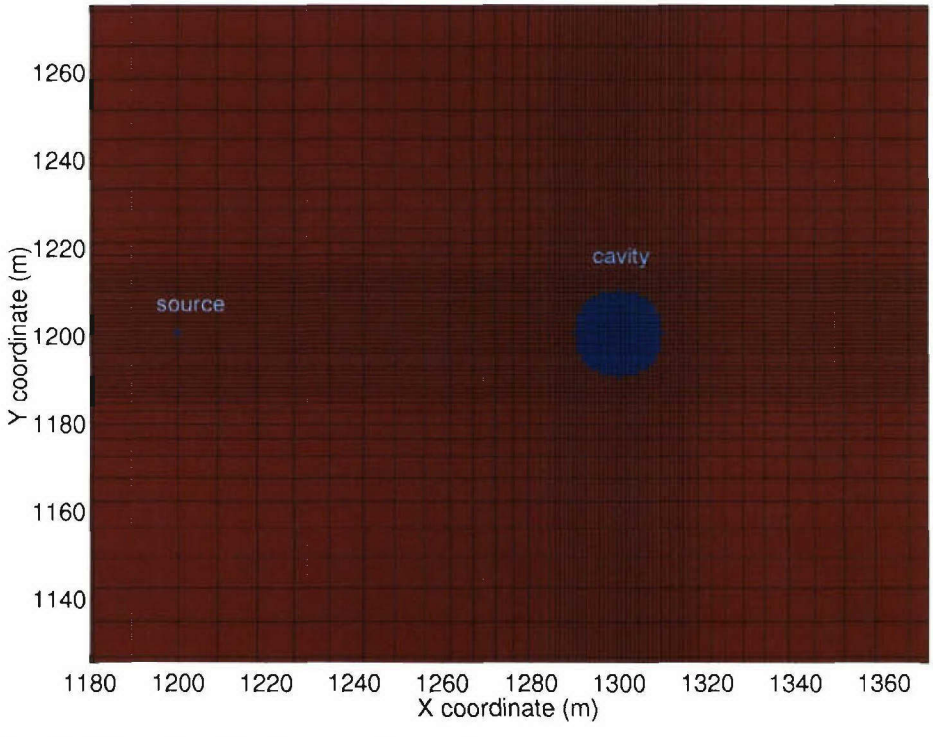

Figure 1b. Griding details close to the cavity.

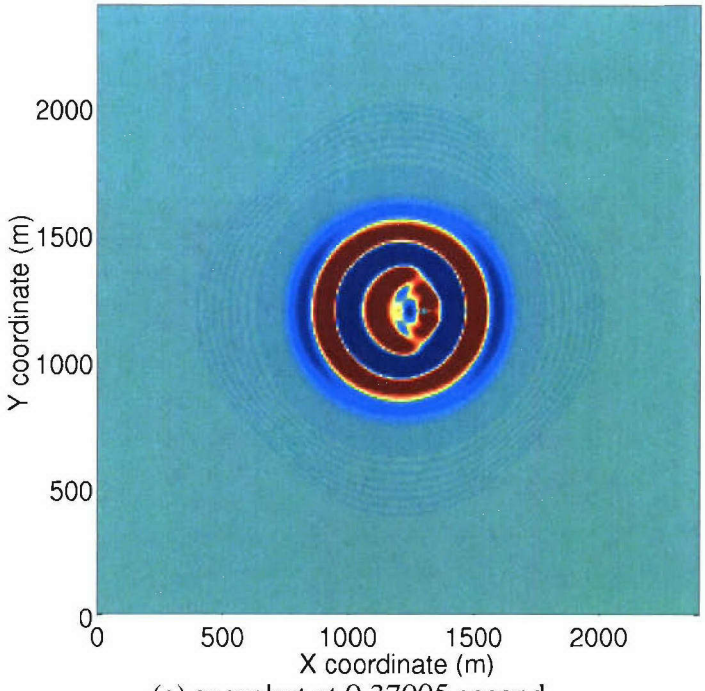

(a) snapshot at 0.37005 second

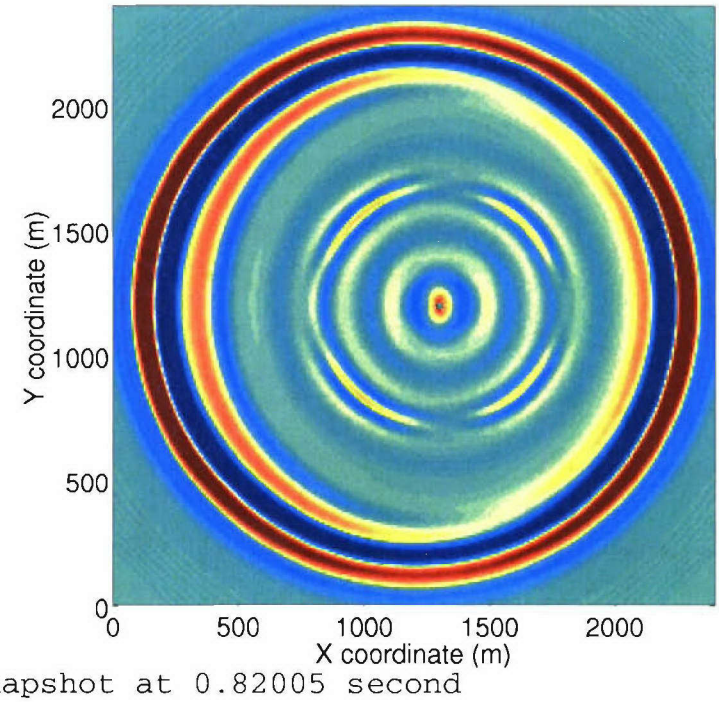

(b) snapshot at 0.82005 second

Figure 2. Snapshot at (a) an early time when the cavity start interfere the source radiation pattern and another one at (b) a later time when both the direct and scattered field are developed. The slice is in the source plane.

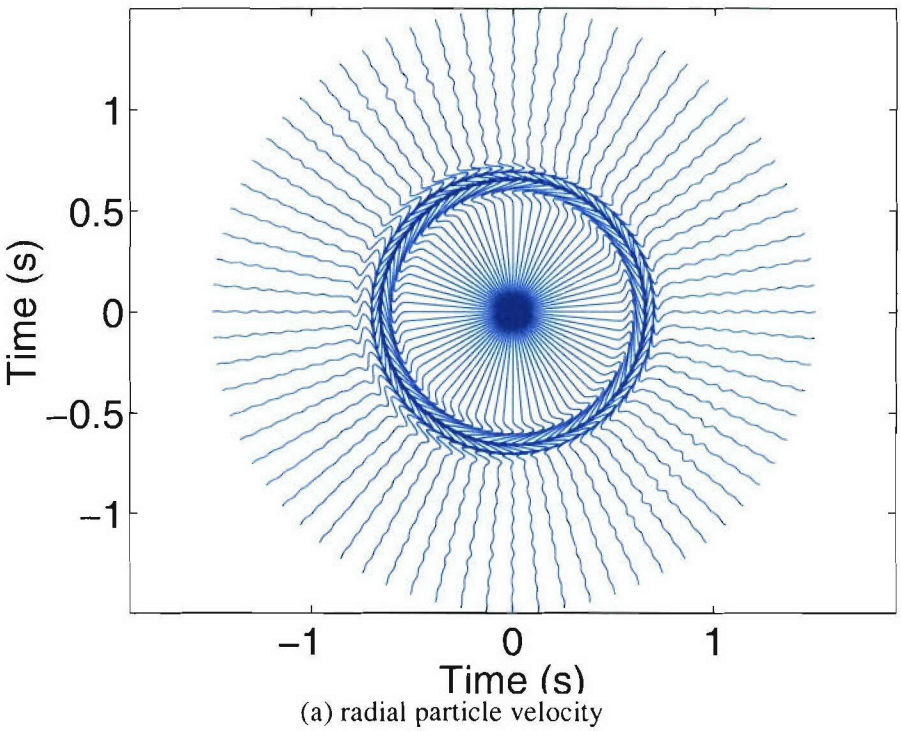

(a) radial particle velocity

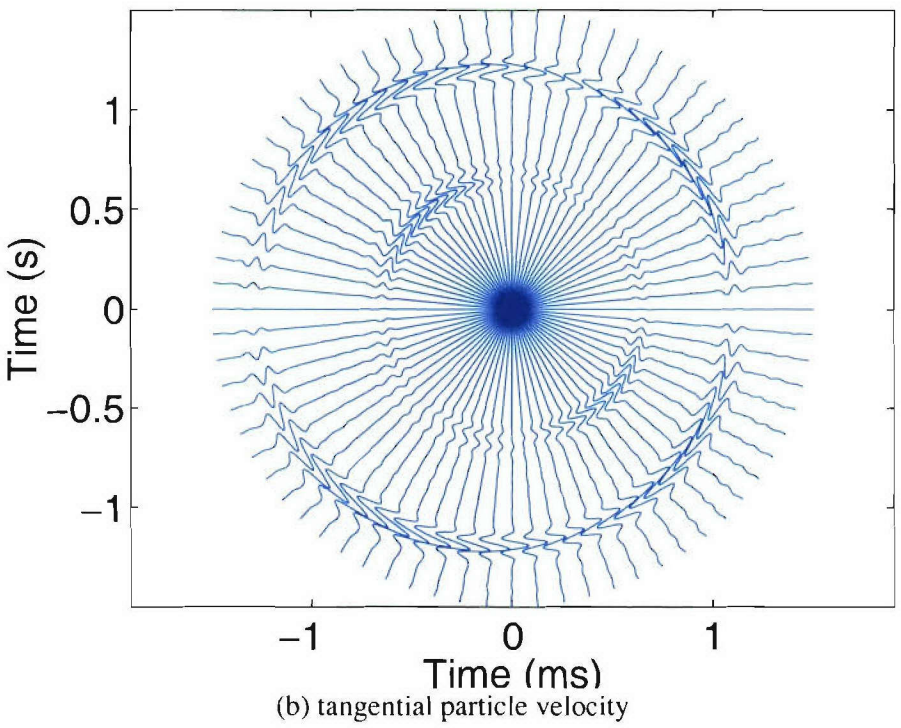

(b) tangential particle velocity

Figure 3. Radial and tangential components of particle velocities at each azimuthal direction. Receivers are 100 m above the source plane.

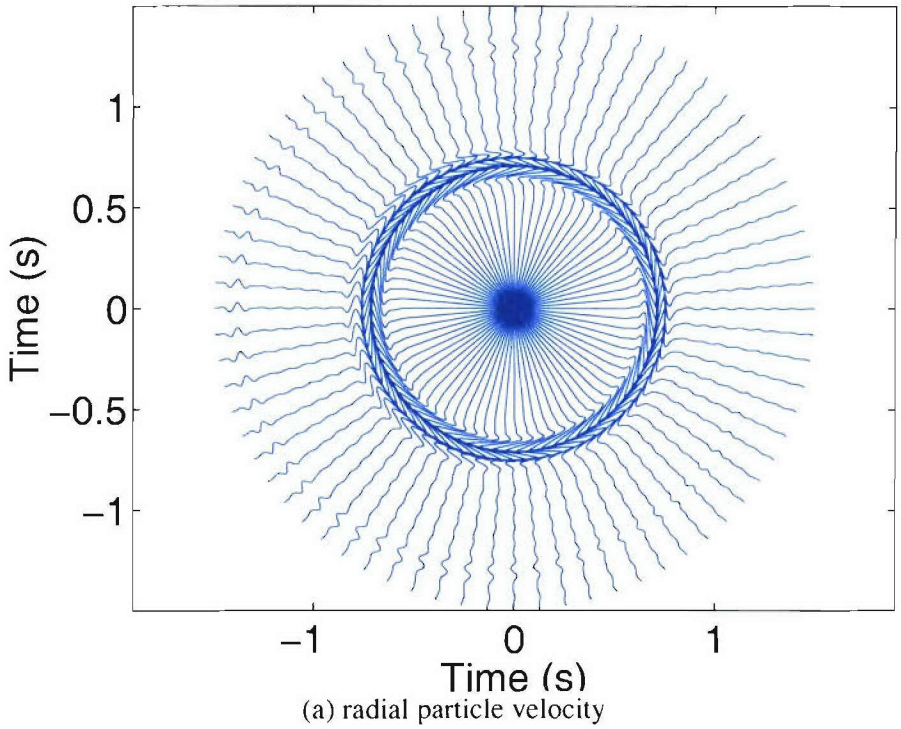

(a) radial particle velocity

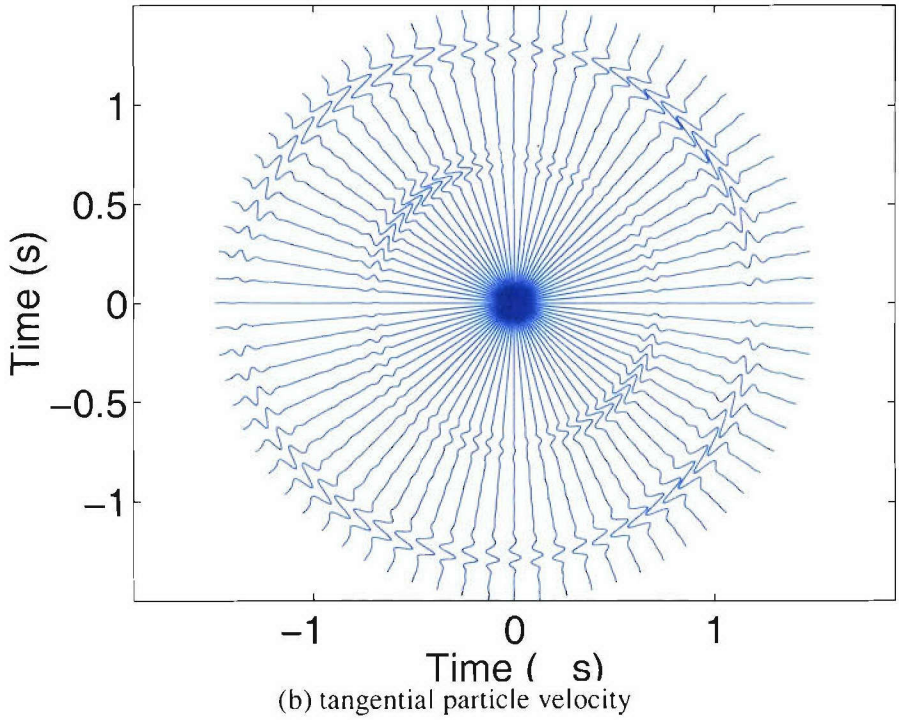

(b) tangential particle velocity

Figure 4. Radial and tangential components of particle velocities at each azimuthal direction. Receivers are 500 m above the source plane.

3.3 Scattering Due to a Near-Source Tunnel in 3-Dimension

Strong scattering from a near-source tunnel is simulated with the FDTD algorithm described above. Figure 5 shows the 3-D geometry of the simulation model in the presence of a cylindrical tunnel.

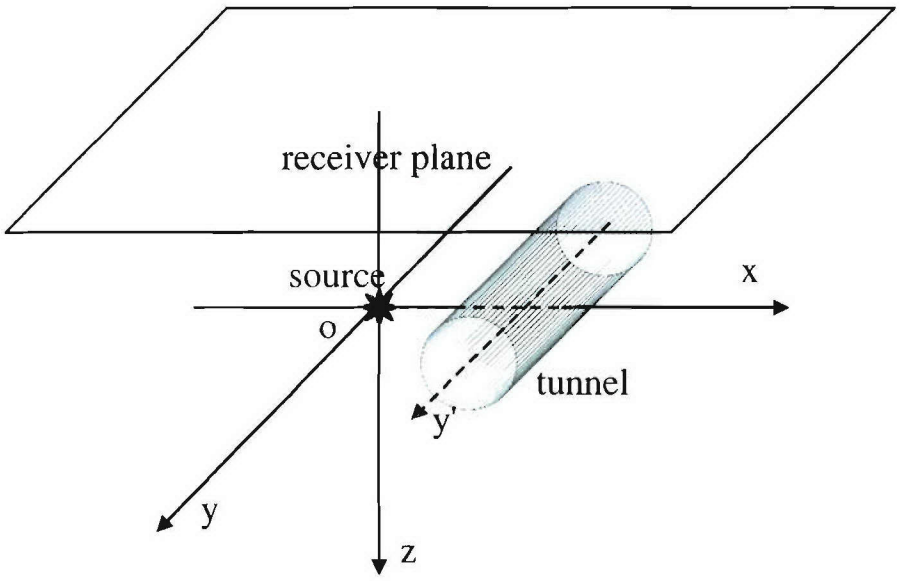

Figure 5. The geometry diagram of the model. The explosion source is set in the middle of the model, coincident with the origin of the coordinates. A cylindrical tunnel is set 30 m away from the source, with radius of 15 m and length of 50 m. Its symmetric axis is parallel to the y axis. The receivers are set in the plane 200 m above the source. The distance between the neighbor receivers is 100 m.

Simulation is also conducted when the tunnel is absent. The infinite formation is modeled by a finite volume of 3000 m by 3000 m by 1100 in the x, y, and z directions. Absorbing boundaries are placed at all six sides of the model to eliminate wave reflection. An explosion source with a center frequency of 40 Hz is excited in the center of the model. The length and radius of the cylindrical tunnel are 50 m and 15 m,

respectively. The axis of the tunnel is parallel to the y axis of the Cartesian coordinate. The distance between the source and the tunnel is 30 m. The formation is a perfect Poisson medium with compressional and shear wave velocities and density of 4000 m/s, 2300 m/s, and 2500 kg/m^3, respectively. Inside the tunnel, we assume a velocity of 340 m/s and a compressed air density of 200 kg/m^3. Grid size increases from 1 m near the source and cylinder tunnel to 10 m away from the source region. Examples of calculated seismograms are shown in Figure 6. The receiver plane is in the XY plane and 200 m above the source. The seismograms are along a line parallel to the X axis. Computations are made for an explosion alone (without a tunnel) and an explosion with a tunnel present.

The first row of Figure 6 shows the x and z components of the motion (velocity fields) when the tunnel is absent. As expected, only P waves are generated. When the tunnel is present near the explosion source, strong scattering occurs. The seismograms in the second row of Figure 6 show that strong shear waves are scattered from the tunnel. To demonstrate the effect of scattering, we subtract the seismograms with an explosion only from those with the explosion plus the tunnel. The third row of Figure 6 shows strong scattered waves. These are both P and S, and scattered S waves are larger than P waves. SH waves are also observed, but their amplitudes are much smaller than the x and z components.

Divergence and curl of the wavefield separate the compressional and shear components of the wavefield. Figure 7 shows the snapshots of the divergence and curl of the velocity field at 60 ms on the XZ, YZ and XY planes passing through the origin of the coordinate system. One can clearly see the complex pattern of the scattering. The curl is zero inside the tunnel. The snapshots of the XZ plane and XY plane reveal the vertical and horizontal cross-section of the tunnel. The snapshot along the YZ plane, parallel to the tunnel, shows the complexity introduced by the finite length of the tunnel.

Understanding the patterns of scattered waves will help us choose appropriate models for inversion of the source mechanism. In the XZ plane, the shear wave energy is divided into four quadrants, and they are in-phase in the diagonal quadrants. Shear waves in the half-space above and below the XY plane are 180° out of phase. Disturbance of

the P wave field due to scattering can also be seen in the divergence field, but the scattering patterns are not as clear as those of the shear waves.

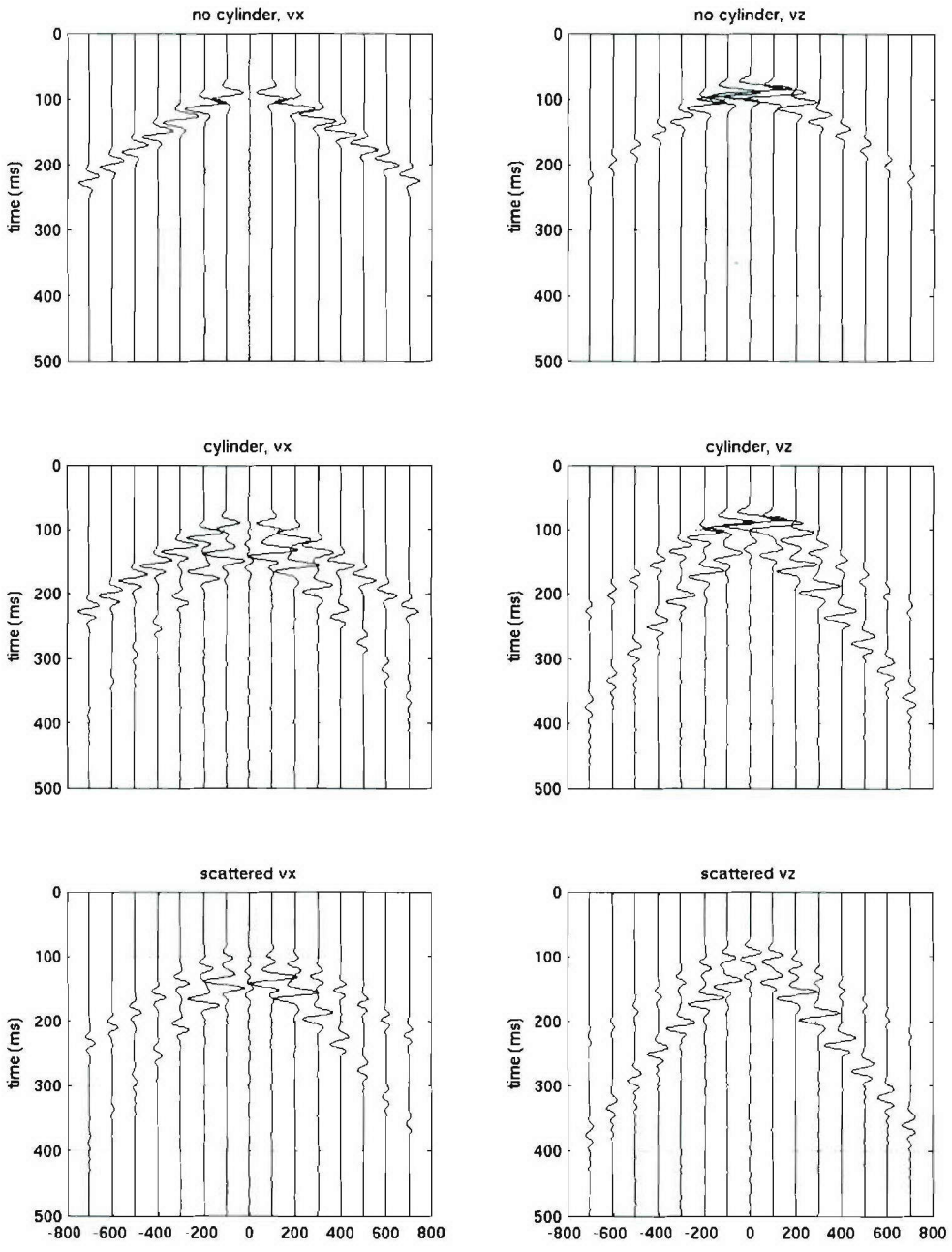

Figure 6: Comparison of the x and z components of the velocity fields at the receiver plane in the absence and the presence of the tunnel. Respective scattered velocity fields of the x and z components are also shown in the last row of this figure.

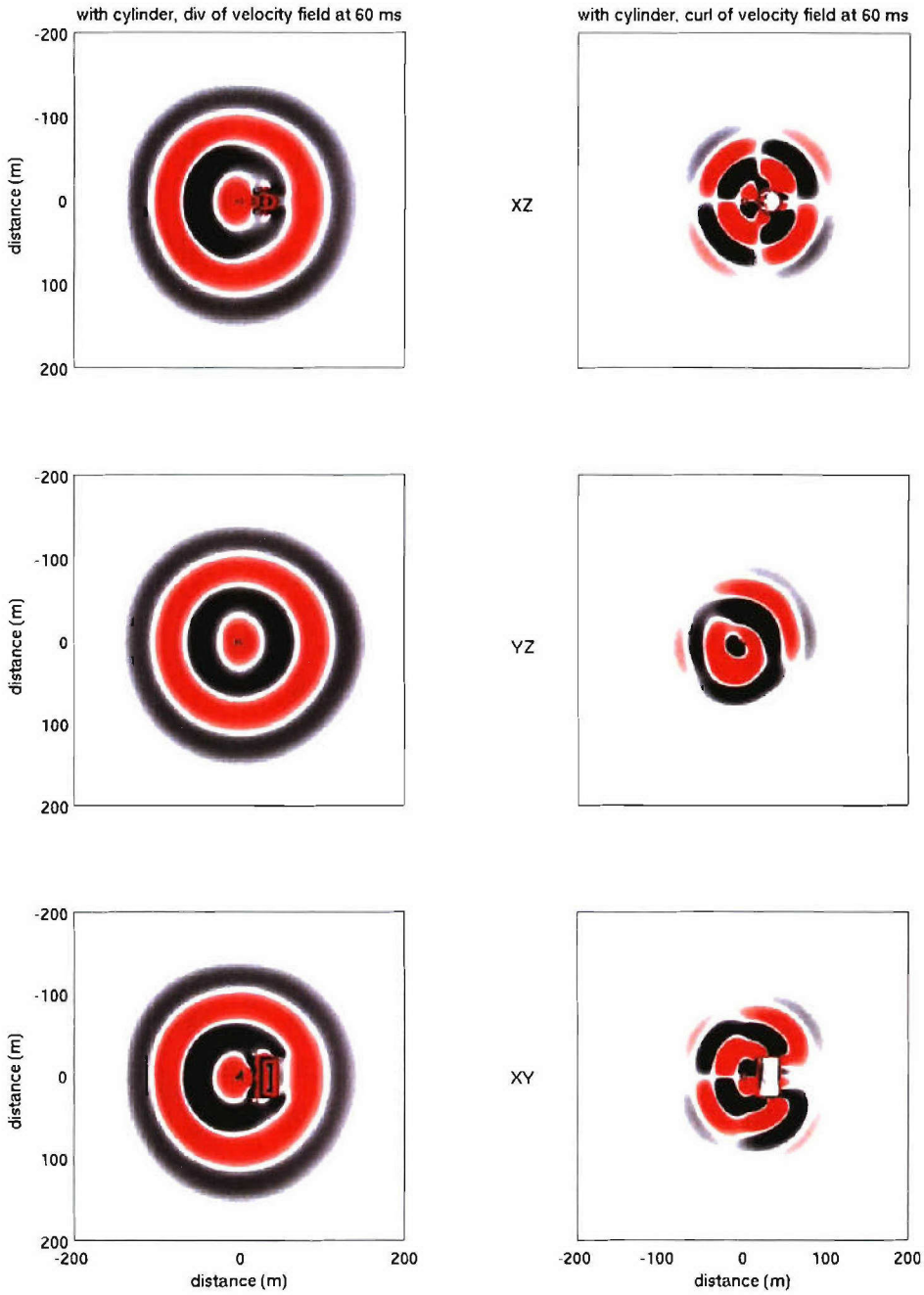

Figure 7: Snapshots of the divergence and curl of the velocity field from an explosion in the presence of a near-source tunnel. The snapshots were taken at 60 ms after the explosion.

The presence of several tunnels creates very complicated scattered waves. Figure 8 shows one example of such a model, where there are six intersecting tunnels, 30 meters below the surface. Two components of the seismic motion are shown.

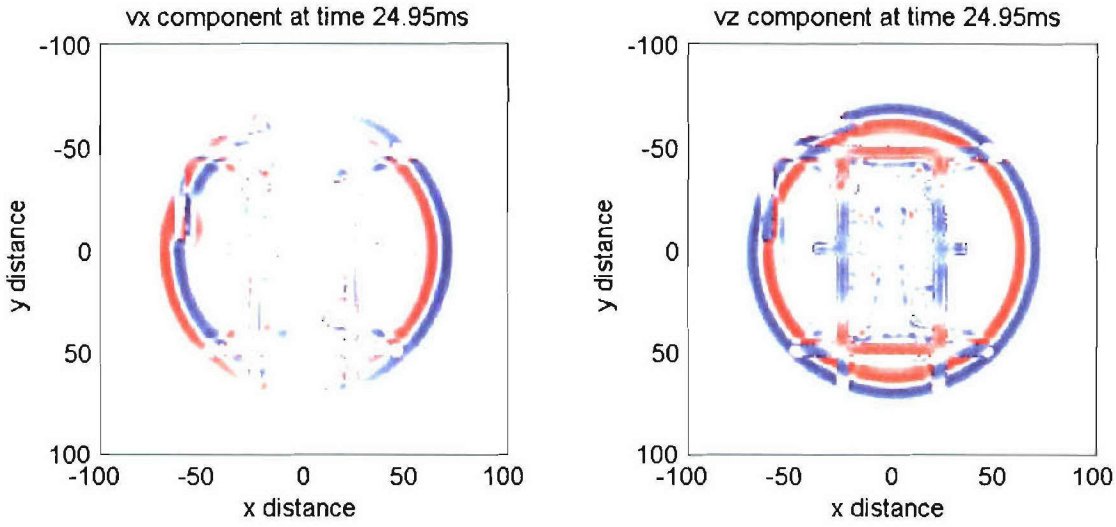

Figure 8: Snapshots of the Vx and Vz components of the velocity field from an explosion in the presence of multiple near-source tunnels. The snapshots were taken at 24.95 ms after the explosion.

3.4 Scattering Modeling Considering Free Surface and Attenuation

We enhanced our modeling ability to realistic earth models that include (1) planar free surface, (2) layered structure, and (3) seismic attenuation. We also incorporated perfectly matched layer (PML) into the finite-difference code to improve the absorption at the boundaries and for memory saving. The program can easily handle arbitrary topography by using a rotated-staggered grid scheme.

3.4.1 Model Description

Strong scattering from a near-source tunnel is simulated with the FDTD algorithm described above. Figure 9 shows the 3-D geometry of the two-layer model with a cylindrical tunnel in the first layer. Simulation is also conducted without the tunnel. The dimensions of the model in the x, y, and z directions are 6,000 m, 6,000 m, and 400 m, respectively. The thicknesses of the first and second layers are 300 and 100 meters, respectively. PML absorbing boundaries are placed at five sides of the model to eliminate wave reflection. The top of the model is the free surface. An explosion source with a center frequency of 10 Hz is placed at 100 m depth. The length and radius of the cylindrical tunnel are 50 m and 15 m, respectively. The axis of the tunnel is parallel to the y axis of the Cartesian coordinates. The distance between the source and the tunnel axis is 55 m.

The elastic properties of the formations and tunnel are as follows. In the first layer, the formation compressional and shear wave velocities and density are 3000 m/s, 1700 m/s, and 2300 kg/m3, respectively. In the second layer, the formation compressional and shear wave velocities and density are 4000 m/s, 2300 m/s, and 2800 kg/m3, respectively. Inside the tunnel, we assume an acoustic velocity of 340 m/s and a compressed air density of 200 kg/m3.

3.4.2 Modeling results—Synthetic seismograms

The receiver array with 100 m spacing forms a dense grid on the free surface. The first row of Figure 10 shows the x and z components of the seismograms along the x axis (velocity fields) when the tunnel is absent. Strong surface waves are observed in both the

x and z components. Due to multiple reflections between the free surface and the layer boundary, P, S, and surface waves are generated and the wavefield becomes extremely complicated. When the tunnel is present near the explosion source, strong scattering occurs. The seismograms in the second row of Figure 10 show that strong surface waves are scattered from the tunnel. To demonstrate the effect of scattering, we subtract the seismograms with an explosion only from those with the explosion plus the tunnel. The third row of Figure 10 shows strong scattered waves. These are surface, P, and S wave; scattered surface and S waves are much larger than P waves. SH waves are also observed in the transverse components.

Figure 11a shows the azimuthal traces when a tunnel is present near the explosion. Figure 11b shows only the scattered wavefields. The forward and backward scatterings are much stronger than in the direction parallel to the tunnel. However, SH components can be observed at all azimuths.

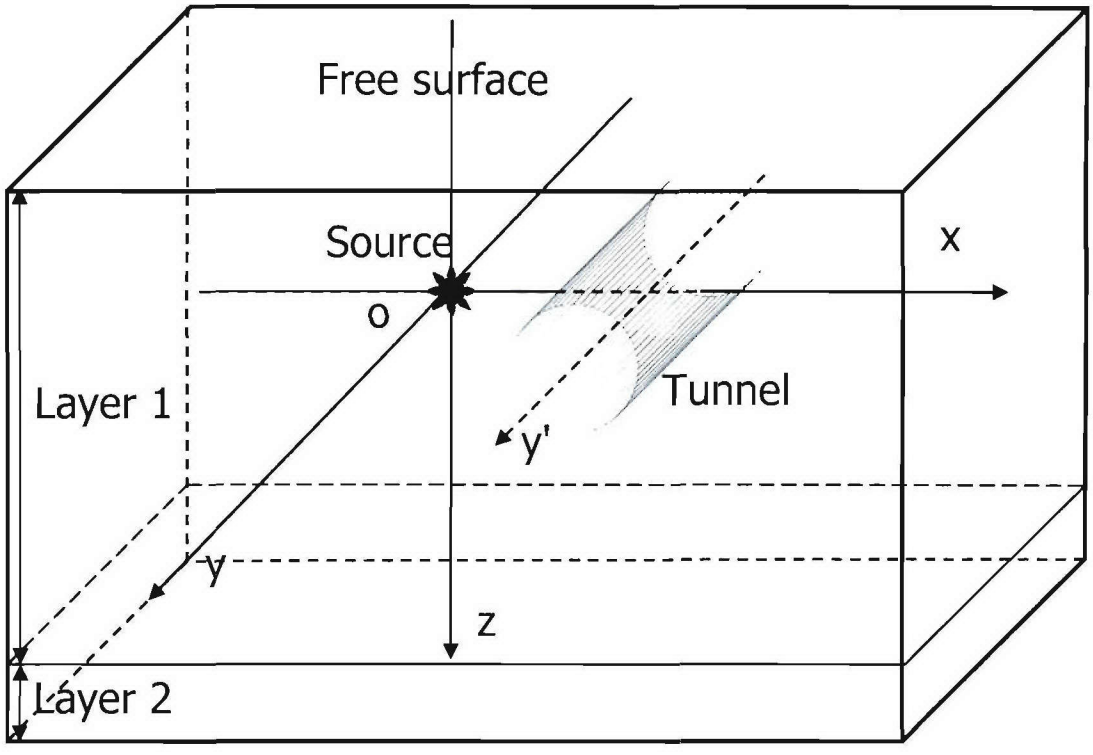

Figure 9: The geometry diagram of the tunnel model. The explosion source is located at 100 meter deep. A cylindrical tunnel is set 30 m away from the source, with radius of 15 m and length of 50 m. Its symmetric axis is parallel to the y axis. The receivers are set on the free surface. The distance between the adjacent receivers in x or y axis direction is 100 m.

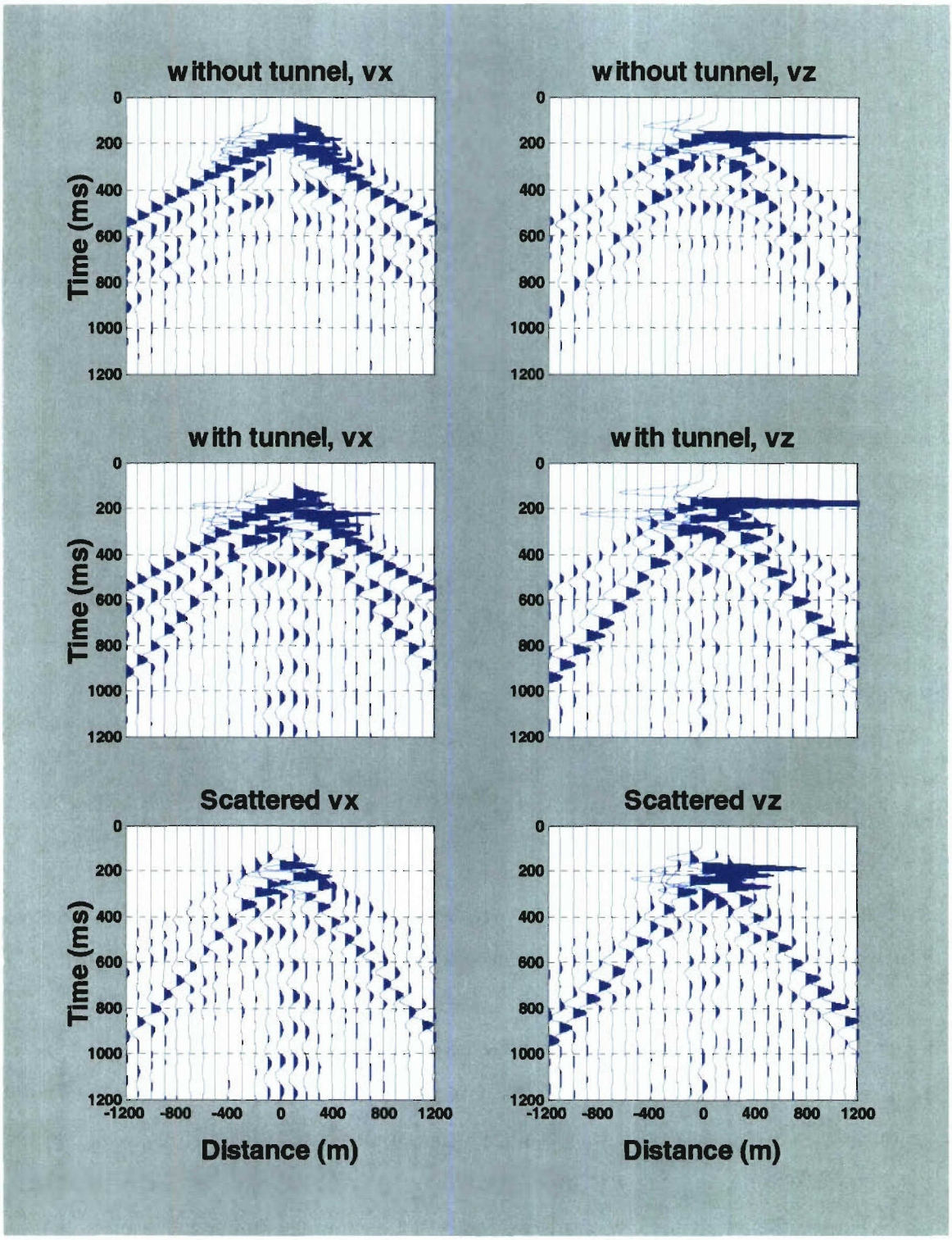

Figure 10: Comparison of the x and z components of the velocity fields at the free surface in the absence and the presence of the tunnel. Respective scattered velocity fields of the x and z components are also shown in the last row of this figure.

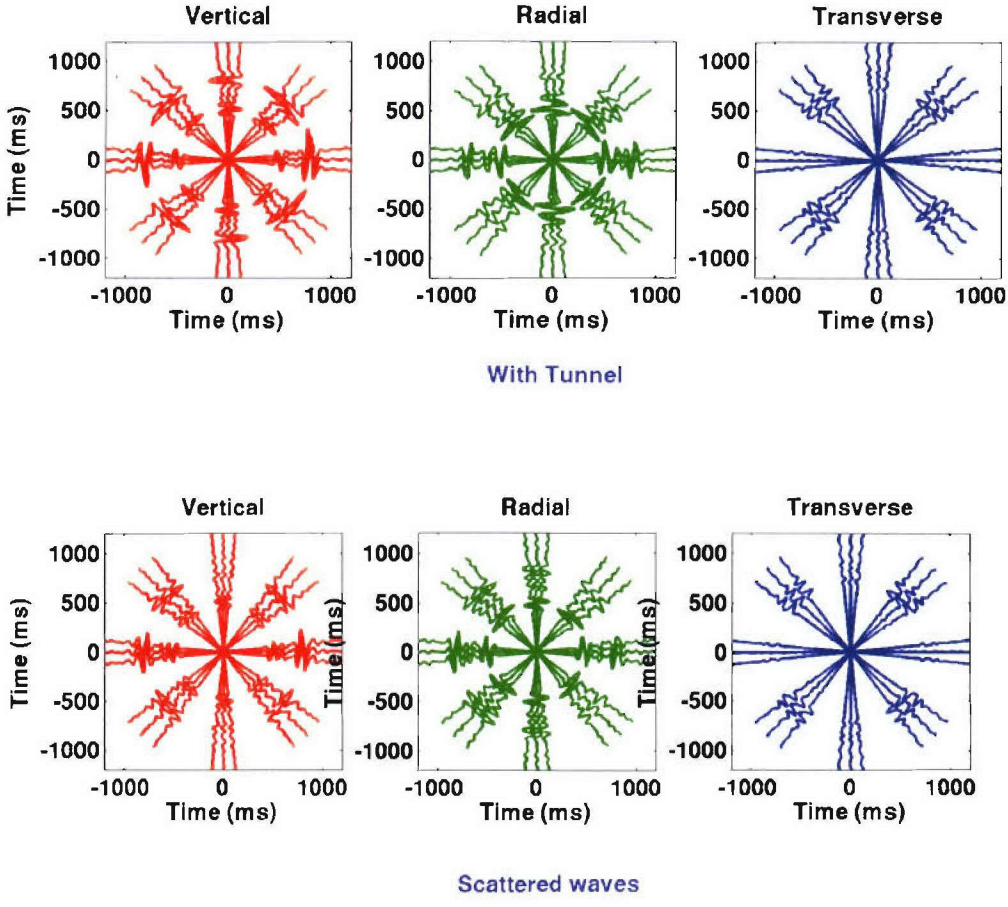

Figure 11: Three components of the recorded wavefields at 1km offset of different azimuths. a) Free surface with tunnel near the explosion. b) Scattered wave only.

3.5 A rotated-staggered grid for finite-difference modeling

We implement a rotated-staggered grid (RSG) for finite-difference modeling. Now the program can easily handle arbitrary topography by using a rotated-staggered grid scheme. The program can also be run on the large scale Alliance for Computational Earth Sciences cluster. It also adopts a perfectly matched layer boundary condition for improved absorption at boundaries of the simulation domain.

We show the capacity of the RSG method in modeling wave scattering due to smooth topography, mesas and canyons. The sharp corners of mesas and canyons act as strong scatters of seismic waves.

3.5.1. Advantages of modeling wave propagation using a rotated-staggered grid

The RSG finite difference has a few remarkable features that are advantageous for modeling an explosion in the vicinity of a high-contrast scatterer, such as tunnels. The differences between the standard-staggered grid (SSG) and the rotated-staggered grid (RSG) are shown in Figure 12.

a. Media with high contrasts in elastic properties

In the standard staggered grid (SSG), all model parameters are located at different positions within a finite difference cell (Figure 12a). In RSG, all components of one physical property, such as stress or elastic moduli, are located at only one location (Figure 12b). Therefore, the RSG method does not average elastic properties, but the SSG method must average the properties. When modeling wave propagation in media with high contrasts in elastic properties, SSG can become inaccurate and unstable, and the RSG method can handle this situation easily.

b. Free surface conditions

In a traditional finite difference algorithm, the free surface boundary condition has to be defined explicitly. When simulating topography at the free surface, one has to use a curvilinear transform of the grid, which makes programming very complicated. In RSG, the properties of air (vacuum) and earth and the free surface are naturally incorporated. In other words, to realize a free surface, we simply set the elastic moduli above the free surface to zero and the density close to zero.

c. Numerical stability and dispersion

The stability is increased by a factor of $\sqrt{3}$ compared to SSG for the velocity-stress RSG method in 3D isotropic media. The SSG has lower dispersion than the RSG by a factor of $\sqrt{3}$. The RSG allows the larger calculation time-step with the same factor.

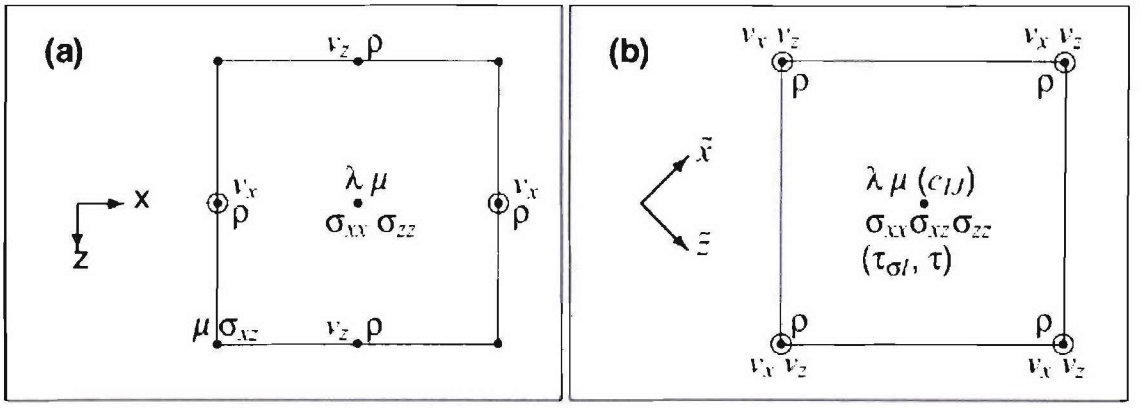

Figure 12. Elementary cells of different staggered grids for a velocity-stress finite difference method. Locations where stress, velocities, and elastic parameters are defined. (a) Velocity-stress finite difference technique using a standard staggered grid. (b) Velocity-stress finite difference technique using the rotated staggered grid. (Saenger and Bohlen, 2004)

Therefore, the newly implemented RSG finite-difference program is a very useful tool to study scattered waves due to near-source tunnels and surface wave scattering due to topography. Applying the RSG technique to a velocity-stress formulation of the wave equation, we can simulate the propagation of seismic waves in the earth considering attenuation.

3.5.2. Scattering due to topography

We study the effects of different topographic features on propagation and scattering of seismic waves from explosion sources at shallow depth. In all the following studies, we use a pressure Kelly wavelet with center frequency of 10 Hz as an explosion source, as shown in Figure 13. The formation compressional and shear wave velocities and density are 3000 m/s, 1700 m/s, and 2300 kg/m^3, respectively.

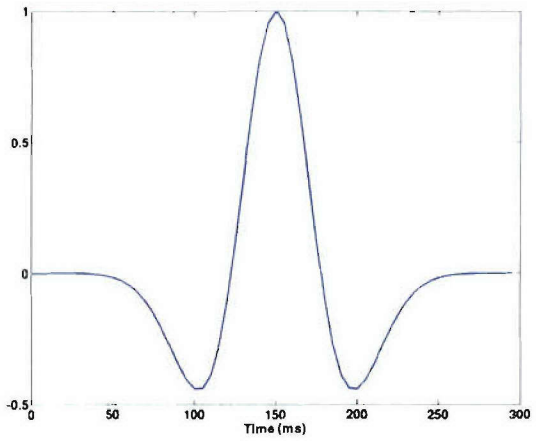

Figure 13. A pressure Kelly wavelet with center frequency of 10 Hz.

a. Scattering due to a hill

We first study the effect of a hill on wave propagation. The hill is 300 m high and 2000 m wide. A tunnel is placed 100 meters below the free surface, as shown in Figure 14. An explosion source with a center frequency of 10 Hz is also placed at the same depth. The length and radius of the cylindrical tunnel are 50 m and 15 m, respectively. The axis of the tunnel is parallel to the y axis of the Cartesian coordinates. The distance between the source and the tunnel axis is 55 m. Inside the tunnel, we assume an acoustic velocity of 340 m/s and a compressed air density of 200 kg/m^3.

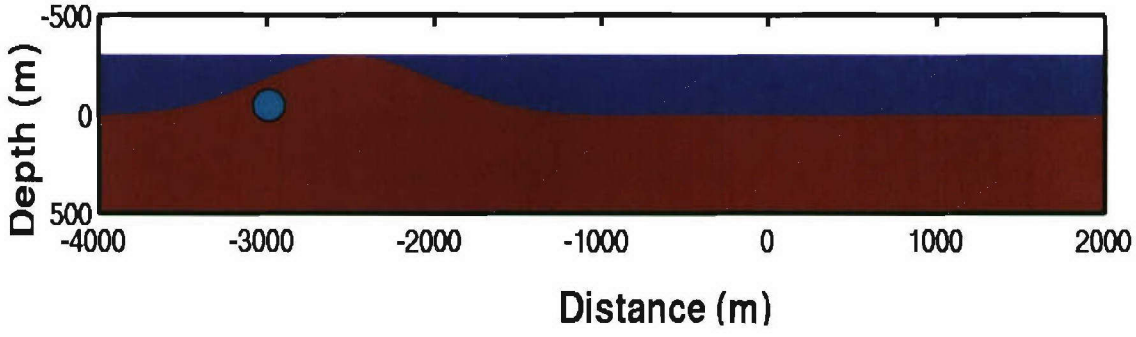

Figure 14. Model for scattering due to a hill.

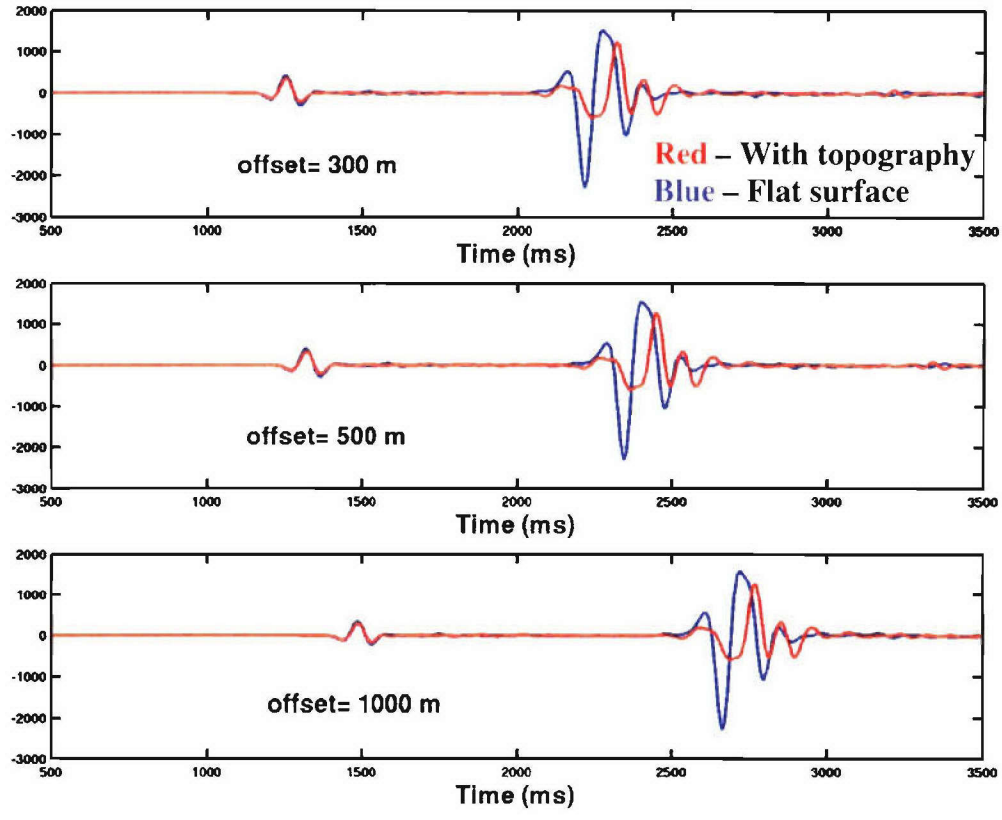

Figure 15. Comparison of waveforms for a flat free surface model and a free surface with a hill.

Figure 15 compares waveforms for a flat free surface model and a free surface with a hill. We see that the presence of the hill does not affect the direct body waves, but affects the surface waves.

b. Scattering due to a canyon

To clearly show the effects of topography on wave propagation, we compare the snapshots of wave fields in earth with a flat free surface (Figure 16a) with those in earth with a canyon and a mesa (Figure 16b,c).

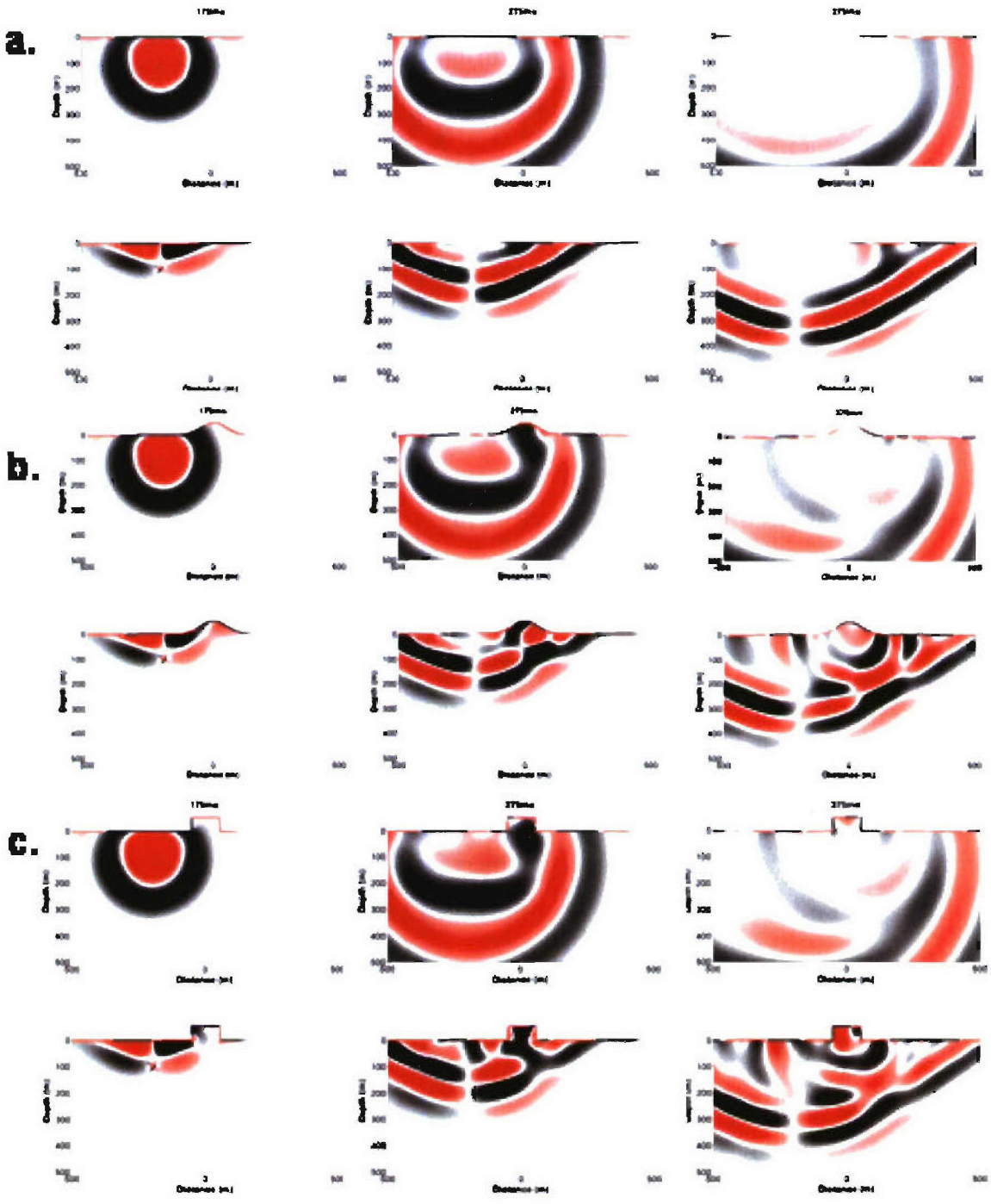

Figure 16. Snapshot of the divergence (upper panel) and curl (lower panel) of the wavefield from an explosion in earth with (a) a flat surface, (b) a canyon, (c) a mesa. Note the strong scattering due to the corners of the features.

We show that the RSG method can effectively model the scattering due to a canyon. The canyon model is 50 m in depth and width. An explosion source with a center frequency of 10 Hz is also placed at 100 m depth and 200 m away from the center of the canyon. Snapshots of the divergence and curl of the wavefield (Figure 16b) show the scattering effects of the sharp corners of the canyon.

c. Scattering due to a mesa

The two-dimensional mesa model is 50 m high and 100 wide. An explosion source with a center frequency of 10 Hz is also placed 100 m below the free surface and 200 m away from the center of the mesa. Divergence and curl of the displacement field separate the compressional and shear components of the wavefield. Figure 16c shows the snapshots of the divergence and curl of the velocity field. Complex patterns of the scattering can be observed due the existence of the free surface and the sharp corners of the mesa.

4. Wavelet-Domain Inversion for Source Parameters

4.1 Review of Moment Tensor Inversion Method

Estimation of the seismic moment tensor and source-time function using waveform inversion has been performed routinely by seismologists to study earthquake mechanisms and source-time histories. Many methods have been developed since Gilbert and Dziewonski (1975) used free oscillation data for their inversion (e.g., Langston, 1981; Kikuchi and Kanamori, 1982; Sipkin, 1982; Nabelek, 1984). Different types of seismic waveforms, such as long-period surface waves (McCowan, 1976; Mendiguern, 1977) and low-frequency body wave data (Stump and Johnson, 1977; Langston, 1981), were inverted for source mechanisms. However, there has been limited success (e.g., Sileny *et al.*, 1992; Sileny and Psencik, 1995; Schurr and Nabelek, 1999) in applying these waveform inversion techniques to high-frequency seismograms, despite widespread availability of broadband three-component data. The waveform inversion methods being used are performed in either the time or frequency domain.

In earthquake mechanism waveform inversions, the most commonly used method to reduce the number of parameters to be determined is using boxcar functions (Langston, 1981) or overlapping triangles (Nabelek, 1984). These parameterization bases sometimes perform poorly in approximating the model (e.g., source-time function, moment tensor rate function, etc.). If these bases failed to represent the model properly, they would give poor estimates of source parameter. Therefore, it is preferable to choose a basis that can construct precise approximations with a linear combination of a small number of vectors selected inside the basis.

4.2 Wavelet-Domain Inversion Method

In this study, we will use a wavelet-based approach to formulate the waveform inversion problem. Wavelet analysis is an increasingly popular tool for numerical studies in signal processing (Mallat, 1989; Wang *et al.*, 1995), biomedical applications (Delaney and Bresler, 1995; Zhu *et al.*, 1997), and geophysics (Deighan and Watts, 1997; Anant and Dowla, 1997; Wood, 1999; Kane and Herrmann, 2001; Kane et al., 2002; Kane, 2003). An extensive description of geophysical applications can be found in Foufoula-Georgiou and Kumar (1995), while a theoretical treatment of wavelet analysis is given by Daubechies (1992), Strang and Nguyen (1997), and Mallat (1998). However, no previous attempt to apply wavelet analysis to earthquake source mechanism inversion has been undertaken. In our proposed method, we adopt a wavelet-based strategy to parameterize the moment tensor rate functions (MTRFs). The MTRFs allow the time-dependent source mechanism such that each moment tensor component has its own time history (Dziewonski and Gilbert, 1974; Stump and Johnson, 1977; Ruff and Tichelaar, 1990; Sileny *et al.*, 1992). By choosing the "best" wavelet as the basis, we can construct an adaptive, problem-dependent parameterization for the MTRFs, thereby achieving accurate approximations while significantly reducing the number of parameters that need to be estimated through inversion. Additionally, we will perform inversion in the wavelet domain rather than the time or frequency domain. This gives the advantage of solving the inverse problem in a multi-resolution sparse matrix representation. We can then solve the problem from coarse to fine levels out to the limit of stability (Sze and Toksöz, 2002). At each resolution level, a regularized least-squares solution is obtained using the

conjugate gradient method. By significantly reducing the number of parameters that need to be estimated, and solving the inverse problem from coarse to fine levels, the wavelet-based method allows us to obtain stable and geologically sensible solutions more easily. Another advantage of transforming the inverse problem to the wavelet domain is that wavelets are powerful tools for denoising data (Donoho, 1993). Transforming data to the wavelet domain tends to isolate signals into a few large-valued coefficients, while the background noise tends to spread around equally with less energy. Therefore, we can incorporate a nonlinear wavelet thresholding operator to remove the small wavelet coefficients, and thus the noise is attenuated with little effect on the signals.

4.3. Example of Wavelet-Domain Inversion Applied to an Explosion and Double-Couple Source

We calculate synthetic seismograms for a combination of an explosion and a double-couple source. Using these we invert for a moment tensor using the wavelet-based method and the conventional time-domain method using overlapping triangular parameterization. We perform two inversion experiments: the first with noise-free data, and the second with correlated white noise. Synthetic data are generated to simulate the case where an explosive source is accompanied by an earthquake with strike-slip mechanism. Figures 17 and 18 show the location of the source and station network. Assuming that the sources of the explosion and the earthquake are at the same place with depth of 0.5 km and have the same source-time function with duration of 0.5 s. We generate synthetic seismograms with a sampling rate of 125 Hz for both the explosive and strike-slip sources using the reflectivity method (Kennett, 1983) and then sum them. We assume that the duration of the MTRFs is one second (125 samples). Results of the inversion (Figure 19) show that the wavelet method has no difficulty in resolving the combined source mechanism. Most importantly, we can obtain a good of MTRFs with only eight wavelet coefficients. In order to compare our wavelet-based method to the conventional method, we repeat the inversion with the same dataset in the time-domain with eight overlapping triangles for parameterization. The results are shown in Figure 20. It can be seen that the conventional method fails to recover a significant amount of the isotropic components of the MTRFs. It also underestimates the magnitude of all the

components. To achieve almost the same accuracy, the conventional time domain method needs 32 overlapping triangles, 4 times that needed by wavelet domain method.

In the second experiment, we evaluate the robustness of the method. We add correlated noise that is simulated by sampling an autoregressive process of order 2. A high noise level is set to be high, with amplitude comparable to the amplitude of the signal. Results obtained from the wavelet-based method and the conventional method are shown in Figures 21 and 22, respectively. With the convenient implementation of the wavelet thresholding technique, the wavelet-based method again outperforms the conventional method and recovers the solution reasonably well. Although the conventional method is able to recover part of the isotropic components of the MTRFs, significant artifacts show up in the latter part of the solution from 0.5 to 1 sec, while again underestimating the magnitude of the MTRFs.

The results obtained using the wavelet-based method show promise. We believe this method can be applied to the understanding of the complexity of source mechanisms associated with a nuclear explosion, and has the ability to resolve the volumetric components from records that are contaminated by earthquakes or secondary sources, such as radiation from strong scatterers.

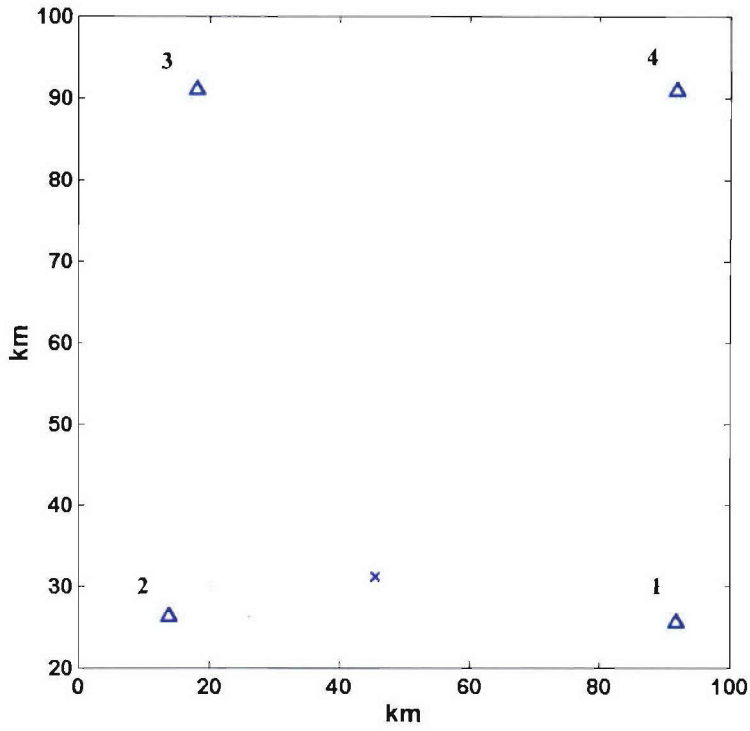

Figure 17. Station positions for the synthetic seismograms. All of them are of regional distances.

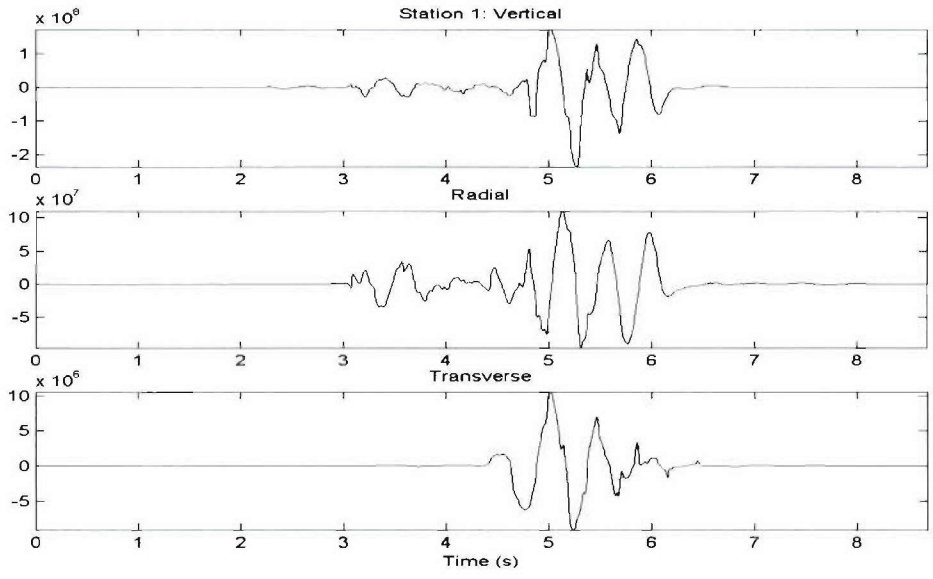

Figure 18. Three-component synthetic seismogram of station 1 generated by reflectivity method. It is obtained by summing two seismograms, one generated by an explosive source and the other by a strike-slip source with a moment tensor component of M_{23}.

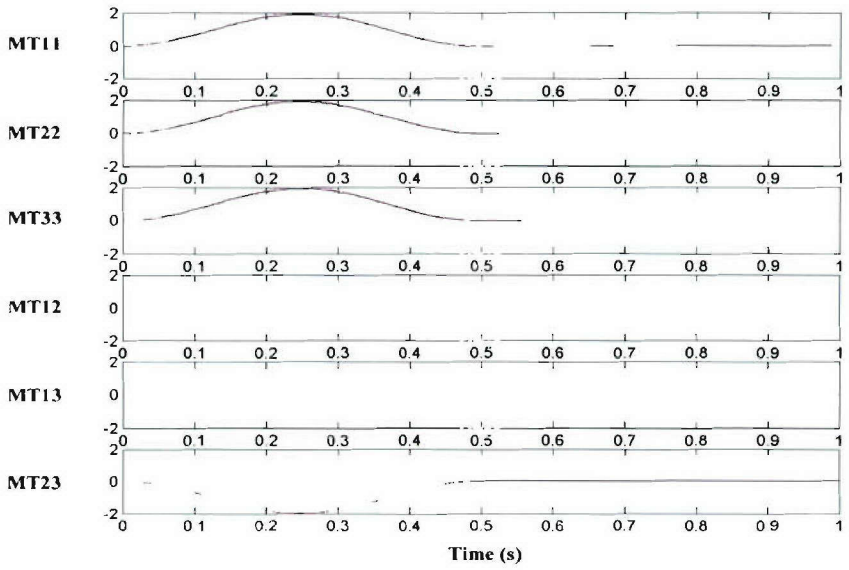

Figure 19. Inversion results of the wavelet-based method on noise-free data. Each trace represent a component of the MTRFs (from top to bottom: the diagonal components MT11, MT22, MT33, and the off-diagonal components MT12, MT13, MT23). The pink lines show the original source-time functions as inputs to the forward modeling. The black lines show the MTRFs recovered by the inversion.

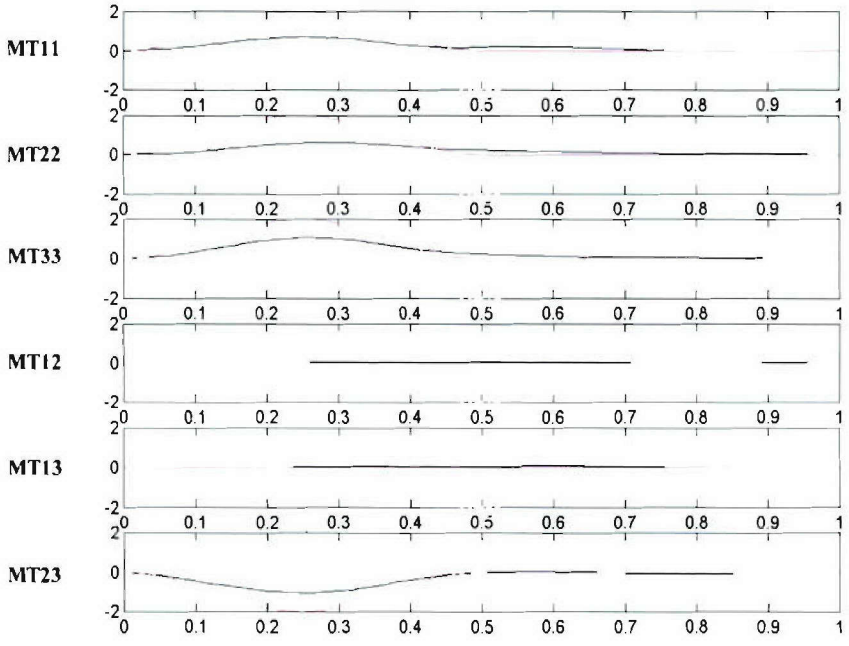

Figure 20. Inversion results of the conventional time-domain method on noise-free data. The pink lines show the original source-time functions as inputs to the forward modeling. The black lines show the MTRFs recovered by the inversion.

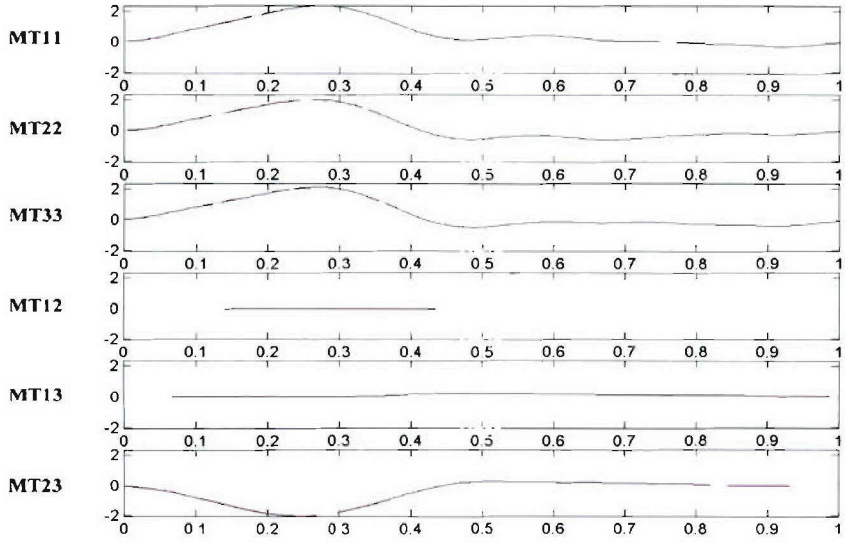

Figure 21. Inversion results of the wavelet-based method on synthetic data contaminated by correlated white noise.

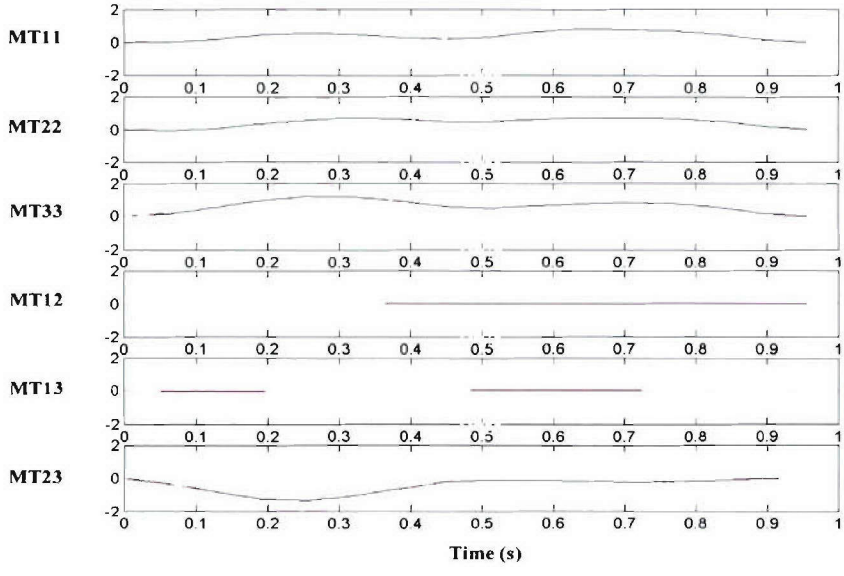

Figure 22. Inversion results of the conventional time-domain method on synthetic data contaminated by correlated white noise.

4.4 Application of Wavelet-Domain Inversion for Explosion near a Tunnel

We use synthetic seismograms to test the performance of the wavelet-domain moment tensor inversion method on seismograms generated by the finite difference

approach. The schematic diagram of the explosion, tunnel and recording plane is shown in Figure 5. This will enable us to evaluate how well our method can resolve the isotropic moment tensor components in the presence of stronger scatter.

Figures 23a and 23b show the results of the wavelet-domain moment tensor inversion and the fitting of the waveforms for the explosion with a tunnel, respectively. The wavelet-domain inversion method was able to retrieve the explosive source mechanism, indicated by the large isotropic components and zero deviatoric components before 0.05 s. The effect of scattering from the tunnel only introduced an anomalous, late shear event at around 0.15 s (Figure 23a) and did not affect our ability to resolve the original explosive mechanism. We obtained good fittings of the synthetic waveforms as well.

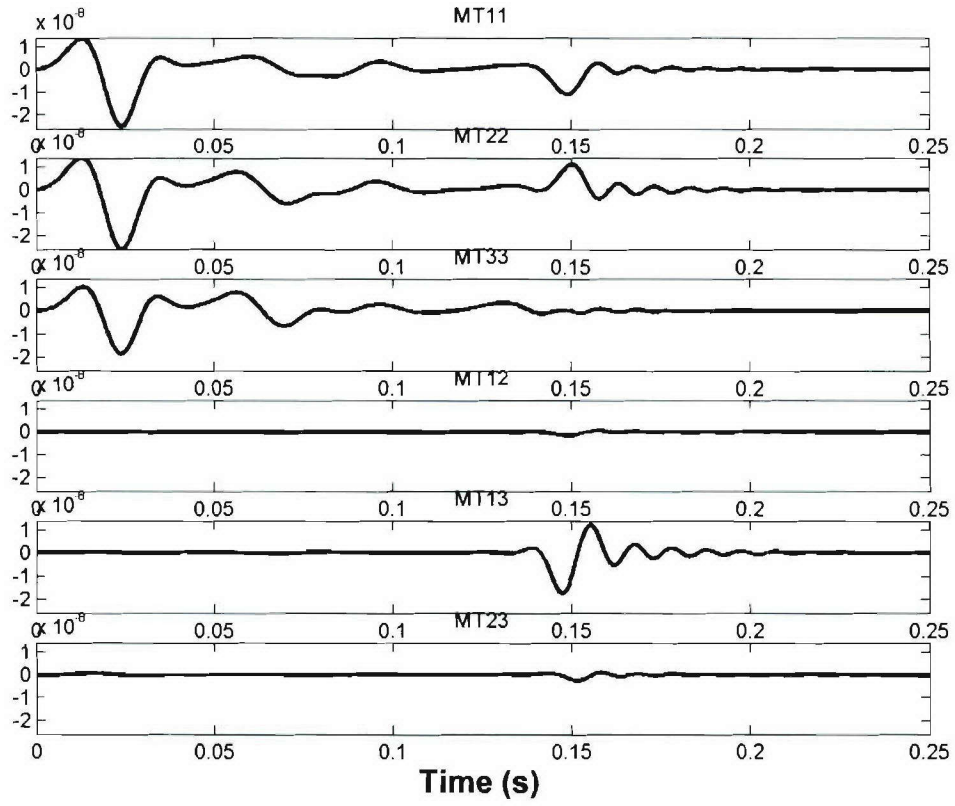

Figure 23a: The results of wavelet-domain moment tensor inversion for an explosion with tunnel. Some anomalous components of M11, M22 and M13 showed up at a later time (~0.15 s) but the inversion was still able to retrieve large isotropic components (M11, M22, M33) and zero deviatoric components (M12, M13, M23) in the beginning.

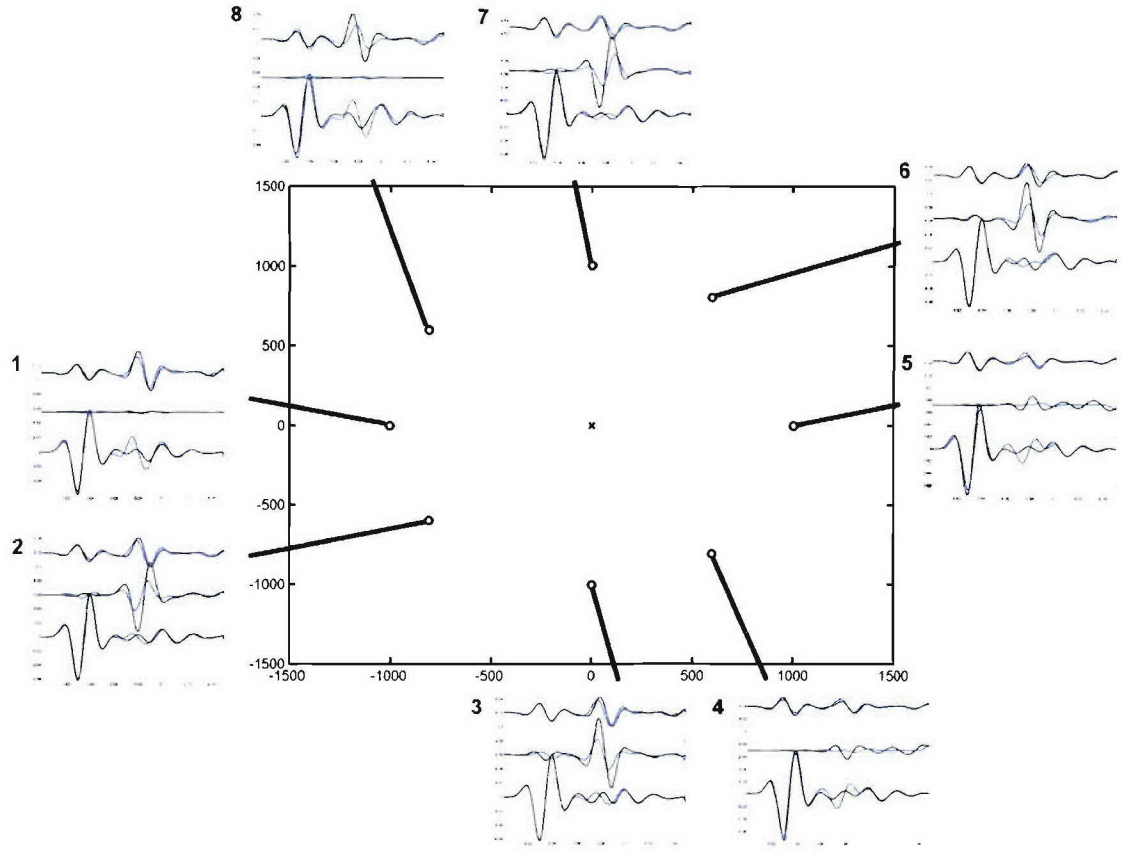

Figure 23b: Fitting of waveforms (blue) by the wavelet-domain inversion to the synthetic data (black) of an explosion with tunnel. Data from eight stations (circles) surrounding the explosion (cross) were used for the inversion. At each station traces are (top to bottom) vertical, tangential and radial components.

5. Source and Scatter Imaging Using Time Reversed Acoustics

5.1 Introduction of Time Reversed Acoustics

According to the TRA concept, acoustic waves recorded at several stations when time-reversed and put back into the medium, propagate and focus at the original source (Fink, 1993, 1999, 2001; Song and Kupperman, 1999; Derode et al., 2000; Lu and Toksöz, 2004). The concept is illustrated schematically in Figures 24a,b. To demonstrate the applicability to seismic source characterization, we conducted two numerical experiments. In each experiment, seismic waves generated by a source in

heterogeneous medium were calculated using the finite difference code. Then these seismograms were time reversed and "pumped" back into the medium.

5.2 Explosion in a layered Homogeneous Medium

Figure 25 shows the geometry of the first experiment where an explosion source is placed in a layered medium and recorded by a circular array of receivers. Note that the source is off-centered. Figure 26 shows, through a series of snapshots, the convergence of the waves to the source.

5.3 Explosion near a Tunnel Buried in a Homogeneous Medium

The next example is for an explosion that is located near a tunnel. A subsurface explosion is modeled by the elastic finite difference code and the seismograms generated are recorded at multiple surface stations. The TRA methodology is applied to these recorded seismograms by first reversing them in time and then applying them as sources at the top of the same 3D elastic modeling algorithm. Figure 27 shows snapshots of the back propagated wave field at four different times. The left column shows the horizontal component of motion, the middle column shows the divergence of the wave field or P wave only energy, and the right column shows the curl of the wave field or the shear wave energy only. The star indicates the location of the source and the circle shows the outline of the tunnel.

The record length of the data used for back propagation was 0.4595 s. The top row of snapshots represent 0.2995 s into the back propagating model which corresponds to 0.160 s in the original forward model time. In a similar fashion, the bottom row of snapshots represent 0.4595 s into the back propagating model or 0.0 s in the original model time. Clearly seen in the bottom row at the original model time is the convergence of the P wave energy at the source position in the left and middle figures. The shear wave energy converges to the tunnel, the source of the P to shear wave conversion, at a back propagation time of 0.4405 s.

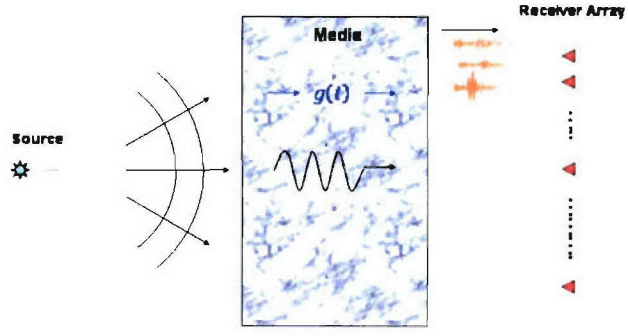

Figure 24a. Schematic showing energy from a seismic source propagating through a medium with many scatterers, and being recorded at the stations denoted by red triangles. The yellow traces represent the recorded seismograms. The recorded traces are created by a convolution of the source function, s(t), with the appropriate transfer function, $g_j(t)$.

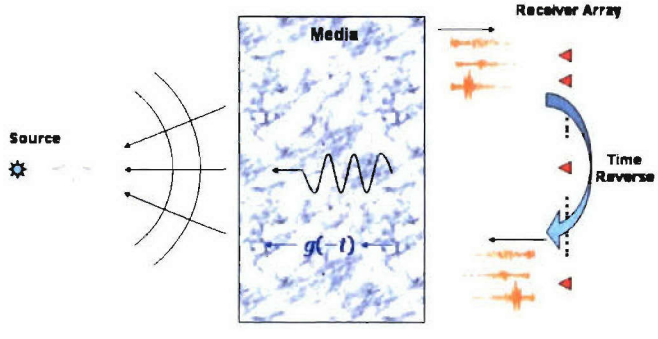

Figure 24b. Schematic showing the TRA process on the data recorded as in Figure 4a. First the recorded seismograms (top yellow traces) are reversed in time (bottom yellow traces) and pumped back into the medium at the station locations. The energy reverses its path through the medium and converges upon the original source position. Due to reciprocity, the Greens function, $g_j(t)$ for each receiver to source path is identical to the source to receiver Greens function.

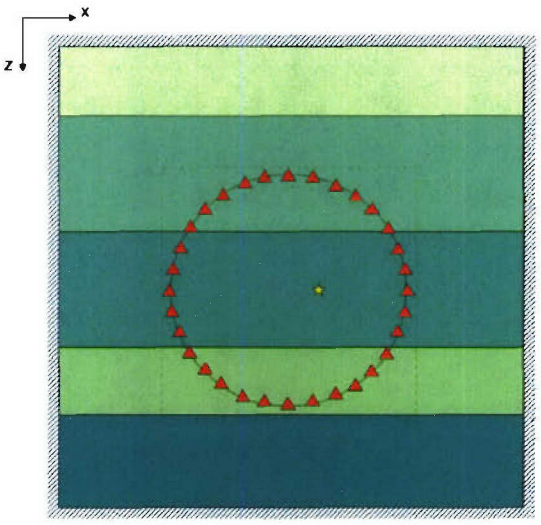

Figure 25. Simple 2D layered earth model with seismic source located at the yellow star, and a ring of receivers, each indicated by a red triangle.

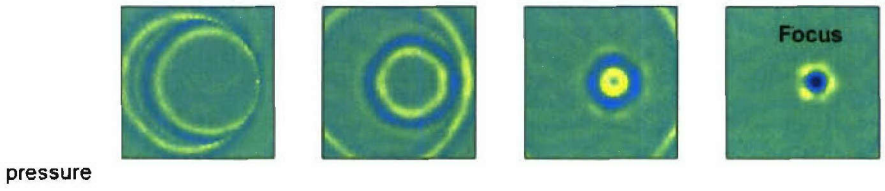

Figure 26. Progressive snap-shots of the wave field propagated backward in time, as originally recorded by the receivers in Figure 25. The fourth column corresponds to zero time in the original, forward model.

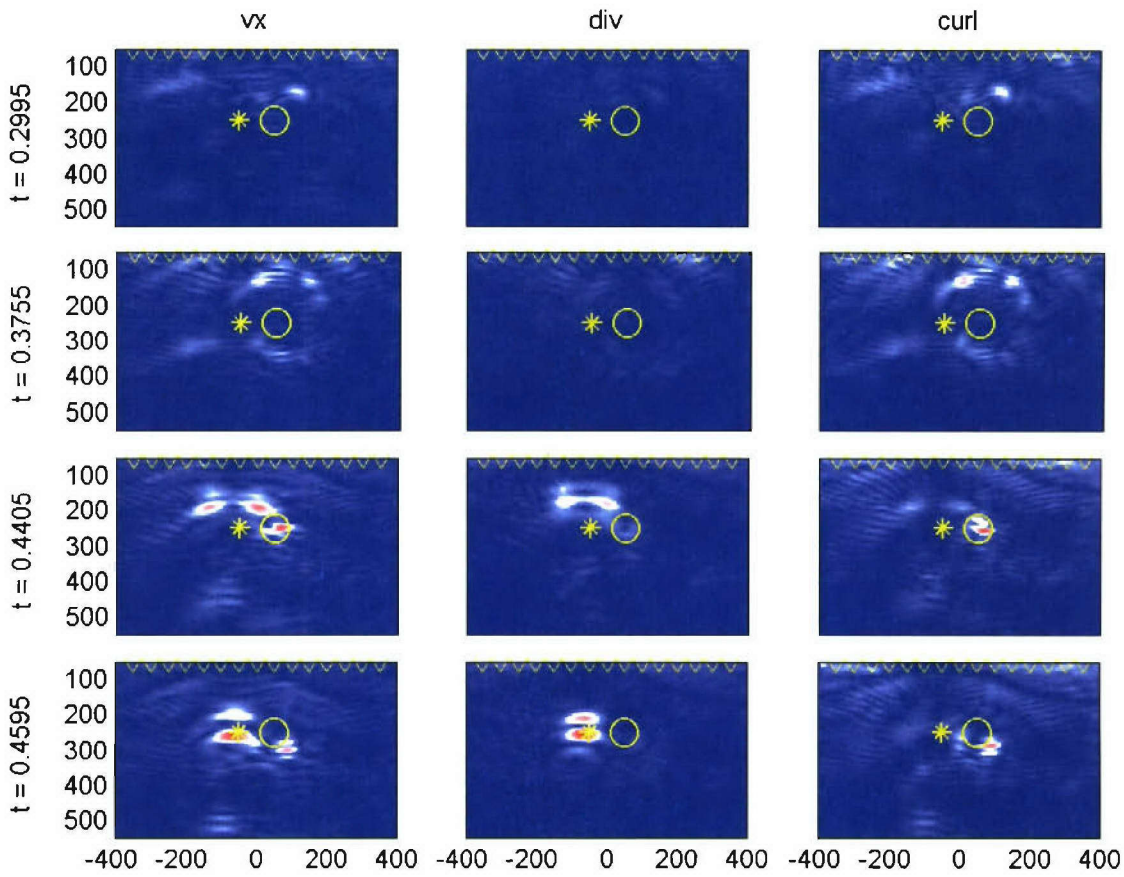

Figure 27. Snapshots of back propagated records for an explosion (star) located next to an air filled tunnel (circle). The left column shows the vertical component of motion, the middle column shows the divergence of the field (P wave energy only), and the right column shows the curl of the field (shear energy only). The bottom row represents zero time in the original forward model.

6. Conclusions and Recommendations

1. A tunnel near an explosion acts as a strong scatterer. P to S scattering is much stronger than P to P scattering. Some energy is scattered into SH waves.

2. Surface topographic features act as scatterers. Overall, scattering from topography is small compared to that of tunnels. The smooth topography effect on scattering is relatively small. Sharp topographic features cause strong scattering of the surface waves.

3. For explosion identification, wavelet-based moment tensor inversion recovers the relative strengths of the explosion and the scatterer source.

4. TRA methodology has the potential of determining seismic source properties with good resolution.

7. References

Anant, K.S. and Dowla, F.U., 1997. Wavelet transform methods for phase identification in three-component seismograms. *Bull. Seism. Soc. Am.*, **87**, 1598–1612.

Archambeau, C. B., and C. Sammis, 1970. Seismic radiation from explosions in prestressed media and the measurement of tectonic stress in the earth. *Rev. Geophys.*, **8**, 473-499.

Ben-Menahem, A., and O. Mikhailov, 1995. Multiple radiation of seismic waves from explosions in non-spherical cavities and its application to signal identification. *J. Acoust. Soc. Am.*, **97**, 5, 2675-2698.

Ben-Menahem, A., 1997. Seismic source functions for explosions in a non-spherical cavity embedded in a scattering environment: application to the regional discrimination of nuclear explosion and earthquakes. *Geophys. J. Int.*, **128**, 97-124.

Browning, G., Kreiss, H.O., and Oliger, J., 1973, Mesh refinement, *Mathematics of Computation, 27*, 29-39.

Crowder, H.J. and Dalton, C., 1971, Errors in the use of nonuniform mesh systems, *J. Computational Physics, 7*, 32-45.

Daubechies, I, 1992. Ten lectures on wavelets. *SIAM*, 357 pp.

Deighan, A.J. and Watts, D.R., 1997. Ground-roll suppression using the wavelet transform. *Geophysics*, **62**, 1896–1903.

Delaney, A.H. and Bresler, Y., 1995. Multiresolution tomographic reconstruction using wavelets. *IEEE Trans. Image Processing*, **6**, 799–813.

Denny, M. D. and S. P. Stull (Editors), 1994. *Proceedings of the Symposium on the Non-Proliferation Experiment (NPE): Results and Implication for Test Bay Treaties*, 19-21 April, Rockville, Maryland, CONF-9404100, Lawrence Livermore National Laboratory, Livermore, California.

Dziewonski, A.M. and Gilbert, F., 1974. Temporal variation of the seismic moment tensor and the evidence of precursive compression for two deep earthquakes, Nature, 247, 185–188.

Fink, M. (1993). Time reversal mirror, J. Phys. D, 26, 1330-1350.

Fink, M. (1999). Time reversed acoustics, Scientific Am., 281, 91-97.

Fink, M. (2001). Time reversed acoustics, Rev. of Progress in Quant. Nondestruct. Eval. 20, 3-15.

Foufoula-Georgiou, E., and Kumar, P. (ed.), 1995. Wavelets in Geophysics. *Academic Press*, 373 pp.

Gibson, R. L., M. N. Toksöz, and W. Dong, 1996. Seismic radiation from explosively loaded cavities in isotropic and transversely isotropic media. *Bull. Seism. Soc. Am.*, **86**, 6, 1910-1924.

Gilbert, F. and Dziewonski, A.M., 1975. An application of normal mode theory to the retrieval of structural parameters and source mechanisms from seismic spectra, *Phil. Trans. R. Soc. A.*, **278**, 187–269.

Gupta, I. N., C. S. Lynnes, T. W. McElfresh, and R. A. Wagner, 1990. F-K analysis of NORESS array and single station data to identify sources of near-receiver and near-source scattering, *Bull. Seismol. Soc. Am.*, ***80***, 2227-2241.

Hayashi, K., 1999, Variable grid finite-difference modeling including surface topography, M.S. thesis, Massachusetts Institute of Technology.

Imhof, M. G. and M. N. Toksöz, 2000. Scattering from tunnels near sources and their effects on seismic signatures of explosions. *Bull. Seism. Soc. Am.*, **90**, 1, 229-242.

Imhof , M. G. and M. N. Toksöz, 2002. The effects of synchronized multiple-cavity sources on seismic radiation. *Bull. Seism. Soc. Am.*, **92**, 6, 2381-2390.

Johnson, L. R., 1995. The effect of near-receiver scattering on seismograms. *In proceedings of 17th Annual Seismic research Symposium on Monitoring a Comprehensive Test Bay Treaty,* J. Lewkowitz (Editor), 12-15 September, Scottsdale, Arizona, Phillips Laboratory, Hanscom AFB, Massachusetts, PL-TR-95-2108, pp. 421-432.

Johnson, L. R., 1997. Generation of S waves by explosion. In M. J. Shore, R. S. Jih, A. Dainty, and Erwin (editors), *proceedings of 19th Annual Seismic research Symposium on Monitoring a Comprehensive Test Bay Treaty,* Defense Special Weapons Agency, 625-631.

Kane, J.A. and Herrmann, F.J., 2001. Wavelet domain inversion with application to well logging, 71st Ann. Int. Mtg. Soc. Expl. Geophys., Expanded Abstracts, 694–697.

Kane, J., F. Herrmann, and M. N. Toksöz, 2002. Wavelet Domain Geophysical Inversion. 72nd Ann. Internat. Mtg., Soc. Explor. Geophys.

Kane, J., 2003. Linear and Nonlinear Solution of Linear Geophysical Inverse Problems. Ph.D. Thesis. Earth Resources Laboratory, Massachusetts Institute of Technology.

Kennett, B.L.N., 1983. Seismic wave propagation in stratified media, *Cambridge University Press*, Cambridge, 339 pp.

Kikuchi, M. and Kanamori, H., 1982. Inversion of complex body waves, *Bull. Seism. Soc. Am.*, **72**, 491–506.

Langston, C.A., 1981 Source inversion of seismic waveforms: the Koyna, India earthquakes of 13 September 1967, *Bull. Seism. Soc. Am.*, **71**, 1–24.

Leavy, D., 1993. Sacttering of elastic waves near an explosion. *Bull. Seism. Soc. Am.*, **83**, 4, 1277-1293.

Lilla, A.D., 1997, Finite difference seismic wave propagation using variable grid sizes, M.S. thesis, Massachusetts Institute of Technology.

Mallat, S., 1989. A theory of multiresolution signal decomposition: The wavelet representation. *IEEE Trans. PAMI*, **11**, 674–693.

Mallat, S., 1998. A wavelet tour of signal processing. Academic Press, 577 pp.

McCowan, D.W., 1976. Moment tensor representation of surface wave sources, *Geophys. J. R. Astr. Soc.*, **44**, 595–599.

Mendiguren, J.A., 1977. Inversion of surface wave data in source mechanism studies, *J. Geophys. Res.*, **82**, 889–894.

Murphy, J. R., I. O. Kitov, J. L. Stevens, D. D. Sultanov, B. W. Barker, N. Rimer, and M. C. Friedman, 1994. Analysis of the seismic characteristics of U.S. and Russian cavity decoupled explosions. Technical Report PL-TR-94-2295 (SSS-DPR-94-14828), Phillips Laboratory.

Nabelek, J., 1984. Determination of earthquake source parameters from inversion of body waves, *PhD thesis*, MIT.

Patton, H. J. and S. R. Taylor, 1995. Analysis of Lg spectral ratios from NTS explosions: Implications for the source mechanisms of spall and the generation of Lg waves, *Bull. Seism. Soc. Am.*, **85**, 220-236.

Pitarka, A., 1999, 3D elastic finite-difference modeling of seismic motion using staggered grids with nonuniform spacing, *Bull. Seismol. Soc. Am., 89*, 54-69.

Priestley, K. F., W. R. Walter, V. Martynov, and M. V. Rozhkov, 1990. Regional seismic recordings of the Soviet nuclear explosion of the joint verification experiment. *Geophys. Res. Lett.*, **17**, 179-182.

Rial, J. A., and B. Moran, 1986. Radiation patterns for explosive-loaded axisymmetric cavities in an elastic medium: analytic approximations and numeric results. *Geophys. J. R. Astr. Soc.*, **86**, 855-862.

Ruff, L.I. and Tichelaar, B.W., 1990. Moment tensor rate functions for the 1989 Loma Prieta Earthquake, *Geophys. Res. Lett.*, **17**, 1187–1190.

Schlittenhardt, J., 1991. The effects of spall on teleseismic P-waves: an investigation with theoretical seismograms. In explosion Source phenomenology, S. Taylor, H. Patton, and P. Richards (editors), American Geophysical Union, Washington, D.C., pp. 141-150.

Schurr, B. and Nabelek, 1999. New techniques for the analysis of earthquake sources from local array data with an application to the 1993 Scotts Mills, Oregon, aftershock sequence, *Geophys. J. Int.*, **137**, 585–600.

Sileny, J., Panza, G.F. and Campus, P., 1992. Waveform inversion for point source moment tensor retrieval with variable hypocentral depth and structural model, *Geophys. J. Int.*, **109**, 259–274.

Sileny, J. and Psencik, I., 1995. Mechanisms of local earthquakes in 3-D inhomogeneous media determined by waveform inversion, *Geophys. J. Int.*, **121**, 459–474.

Sipkin, S., 1982. Estimation of earthquake source parameters by the inversion of waveform data: synthetic waveforms. *Phys. Earth. Planet. Inter.*, **30**, 242–259.

Stevens, J. L, J. R. Murphy, and N. Rimer, 1991. Seismic source characteristics of cavity decoupled explosions in salt and tuff. *Bull. Seism. Soc. Am.*, **81**, 4, 1272-1291.

Stump, B.W. and Johnson, L.R., 1977. The determination of source properties by the linear inversion of seismograms, *Bull. Seism. Soc. Am.*, **67**, 1489–1502.

Stump, B. W., R. E. Reinke, K. H. Olson, and L. R. Johnson, 1994. Isotropic and deviatoric characterization of the Coalora nuclear explosion in Yucca Flats. *Geophys. J. Int.*, **116**, 538-552.

Strang, G. and Nguyen, T., 1997. Wavelets and filter banks. Wellesley-Cambridge Press, 520 pp.

Sze, E. K. M., and M. N. Toksöz, 2002. Wavelet-domain regularized least-squares inversion for earthquake source parameters (abstact). 74th Annual Meeting of the Eastern Section of the Seismological Society of America. *Seism. Res. Lett.*, 74, 1, pp68.

Tadeu, A. J. B., E. Kausel, and C. Vrettos, 1996. Scattering of waves by subterranean structures via the boundary element method. *Soil Dynamics and Earthquake Engineering*, 15, 387-397.

Toksöz, M. M., D. G. Harkrider, and A. Ben-Menahem, 1965. Determination of source parameters by amplitude equalization of seismic surface waves: Part 2, Release of tectonic strain by underground nuclear explosions and mechanisms of earthquakes, *Journ. Geophys. Res.*, **70**, 907-922.

Toksöz, M. N., and H. H. kehrer, 1972. Tectonic strain release by underground nuclear explosions and its effect on seismic discrimination. *Geophys. J. R. astr. Soc.*, **31**, 141-161.

Toksöz, M. N., S. Juleli, C. Schultz, D. Harris, C. Gurbuz, D. Kalafat, and A. Isikara, 2002. Calibration of regional seismic stations in the Middle East with shots in Turkey. *Proceedings of 24th Annual Seismic research Review--Nuclear Explosion Monitoring: Innovation and Integration—September 17-19, 2002, 200-208.,*

Wallace, T. C., D. V. Helmberger, and G. R. Engen, 1983. Evidence of tectonic release from underground nuclear explosions in long-period P-waves, *Bull. Seism. Soc., Am.*, **73**, 593-613.

Wallace, T. C., D. V. Helmberger, and G. R. Engen, 1985. Evidence of tectonic release from underground nuclear explosions in long-period S-waves, *Bull. Seism. Soc., Am.*, **75**, 157-174.

Wang. G., Zhang, J. and Pan G., 1995. Solution of inverse problems in image processing by wavelet expansion. *IEEE Trans. Image Processing*, **4**, 579–593.

Wood, W., 1999. Simultaneous deconvolution and wavelet inversion as a global optimization. *Geophysics*, **64**, 1108–1115.

Zhao, L., and D. G. Harkrider, 1992. Wavefields from an off-center explosion in an embedded solid sphere. *Bull. Seism. Soc. Am.*, **82**, 1927-1955.

Zhu, W., Wang, Y., Deng, Y, Yao, Y. and Barbour, R., 1997. A wavelet-based multiresolution regularized least squares reconstruction approach for optical tomography, *IEEE Trans. Medical Imaging*, **16**, 210–217.